

A SPECTROSCOPIC CATALOG OF THE BRIGHTEST ($J < 9$) M DWARFS IN THE NORTHERN SKY

SÉBASTIEN LÉPINE^{1,2}, ERIC J. HILTON^{3,4}, ANDREW W. MANN³, MATTHEW WILDE¹, BÁRBARA ROJAS-AYALA¹, KELLE L. CRUZ^{1,2,5},
& ERIC GAIDOS⁴

Submitted to The Astronomical Journal

ABSTRACT

We present a spectroscopic catalog of the 1,556 brightest M dwarf candidates in the northern sky, as selected by proper motion and photometry. These bright sources comprise $> 99\%$ of the known, northern M dwarfs with apparent magnitudes $J < 9$, and most likely include $> 95\%$ of all such existing objects. Only 679 stars in our sample are listed in the Third Catalog of Nearby Stars (CNS3); most others are relative unknowns and have spectroscopic data presented here for the first time. Observations confirm 1,403 of the candidates to be late-K and M dwarfs with spectral subtypes K7-M6, with subtypes assigned based on spectral index measurements of CaH and TiO molecular bands. We find that spectral band index measurements are dependent on spectral resolution and spectrophotometric calibration, and must be calibrated and corrected for each observatory/instrument used. After systematic corrections and a recalibration of the subtype-index relationships for the CaH2, CaH3, TiO5, and TiO6 spectral indices, we find that we can reliably classify all our stars to a half-subtype precision. We then calculate the ζ parameter, which measures the ratio of TiO and CaH bandheads, and is correlated with metallicity in M dwarfs/subdwarfs, and for this we present a revised calibration based of our corrected values of the CaH and TiO spectral indices. We find that our ζ values are not accurate enough to diagnose metallicity variations in our sample for subtypes M2 and earlier ($\pm 0.5\text{dex}$ accuracy) and are only marginally useful at later M3-M5 subtypes ($\pm 0.2\text{dex}$ accuracy). Fits of our spectra to the Phoenix atmospheric model grid are used to estimate effective temperatures; these suggest the existence of a plateau in the M1-M3 subtype range, in agreement with model fits of infrared spectra but at odds with photometric determinations of T_{eff} . Existing geometric parallax measurements for 624 of the catalog stars are used to recalibrate the subtype/absolute magnitude relationship in M dwarfs; we find that spectroscopic distances are marginally more accurate at earlier (K7-M2) subtypes, but that photometric distances should be preferred for later-type dwarfs (M3-M6). We identify active stars from measurements of H α equivalent widths, which are compared to near-UV magnitudes from GALEX and X-ray fluxes from ROSAT; a strong correlation is observed between H α emission in M dwarfs and a strong X-ray and/or UV excess. We combine proper motion data and photometric distances to evaluate the distribution in (U,V,W) velocity space of the entire catalog. The overall velocity-space distribution correlates tightly with the velocity distribution of G dwarfs in the Solar Neighborhood. However, active stars show a smaller dispersion in their space velocities, which is consistent with those stars being younger on average. Our catalog will be most useful to guide the selection of the best M dwarf targets for exoplanet searches, in particular those using high-precision radial velocity measurements.

Subject headings: stars: low-mass, brown dwarfs – stars: late-type – surveys – catalogs – stars: fundamental parameters – stars: activity

1. INTRODUCTION

M dwarfs are now among the targets of choice of many exoplanet surveys. This is because low-mass planets (i.e. Earth-to Neptune-size) are easier to detect by the Doppler or transit techniques around lower mass stars. The transits of smaller planets are also easier to detect when they occur in the smaller M dwarfs. In addition, M dwarfs have much lower luminosities than the Sun, and their “habitable zones” (HZ) are closer in, which makes transits more likely to occur and radial ve-

locity variations easier to detect. Earth-like planets within the habitable zones of M dwarfs are thus eminently more detectable with current observational techniques than those around G dwarfs (Tarter et al. 2007; Gaidos et al. 2007).

M dwarfs are also the most plentiful class of stars, constituting a significant fraction ($> 70\%$) of main sequence objects in the Galaxy and in the vicinity of the Sun (Reid, Gizis, & Hawley 2002; Covey et al. 2008; Bochanski et al. 2010). However, even nearby M dwarfs are generally faint at the visible wavelengths where most planet searches are conducted, and most exoplanet detection techniques – with the notable exception of micro-lensing (Dong et al. 2009) – are currently restricted to the brightest stars. This has limited the number of M dwarfs targeted in exoplanet surveys. Doppler searches in particular are usually restricted to stars with visual magnitudes $V < 12$, and less than $\sim 10\%$ of late K and early M stars within 30 pc are currently being monitored by the large-scale Doppler surveys (Butler et al. 2006; Mayor et al. 2009). However, new surveys are pushing this limit (Apps et al. 2010) to fainter magnitudes, and high-resolution spectrographs suitable for Doppler ob-

¹ Department of Astrophysics, American Museum of Natural History, Central Park West at 79th Street, New York, NY 10024, USA; lepine@amnh.org, brojas-ayala@amnh.org, mwilde@amnh.org, mshara@amnh.org

² Department of Physics, Graduate Center, City University of New York, 365 Fifth Avenue New York, NY 10016, USA

³ Institute for Astrophysics, University of Hawai‘i, Honolulu, HI 96822, USA; hilton@ifa.hawaii.edu, amann@ifa.hawaii.edu

⁴ Department of Geology & Geophysics, University of Hawai‘i, 1680 East-West Road, Honolulu, HI 96822, USA; gaidos@hawaii.edu

⁵ Department of Physics and Astronomy, Hunter College, City University of New York, 695 Park Avenue, New York, NY 10065, kelle-cruz@gmail.com

servations at near-infrared wavelengths, where M dwarfs are relatively brighter, are being introduced (Terada et al. 2008; Bean et al. 2010; Quirrenbach et al. 2010; Wang et al. 2010). Transit surveys, on the other hand, can include much fainter stars (Irwin et al. 2009) albeit with much lower detection efficiency due to orbital inclination constraints.

A fundamental obstacle to progress has been the lack of a large, uniform catalog of bright M dwarfs suitable as targets. The Hipparcos catalog is complete only to $V < 8$ has a visual magnitude limit $V < 12$ (van Leeuwen 2007), which excludes all but the nearest M dwarfs. The widely utilized *Third Catalog of Nearby Stars*, or CNS3 (Gliese & Jahreiss 1991), which lists $\approx 3,800$ stars and extends to fainter visual magnitudes, has been largely used in recent years to select M dwarf targets for exoplanet surveys, but the catalog suffers from various sources of incompleteness, as demonstrated by the large number of nearby M dwarfs newly identified in recent proper motion surveys (Lépine 2005; Reid, Cruz, & Allen 2007; Lépine 2008; Boyd et al. 2011). In order to provide a more complete list of bright M dwarfs, we have searched the current list of $\mu > 40$ mas yr $^{-1}$ stars from the SUPERBLINK proper motion survey, and compiled an all-sky catalog of 8,889 bright ($J < 10$) M dwarfs candidates (Lépine & Gaidos 2011). Of these, we found that only 982 were previously listed in the Hipparcos catalog, and another 898 in the CNS3. Most of the other 7009 stars were not commonly known objects, and were identified as probable nearby M dwarfs for the first time.

Not all M dwarfs, however, are equally suitable targets for planet searches. Some M dwarfs have significant photometric variability (flares, spots) which affecting transit searches (Hartman et al. 2011). Some display chromospheric emission affecting Doppler searches (Isaacson & Fischer 2010). Because M dwarfs are relatively faint stars, they often require considerable investment of observing time on large telescopes to achieve exoplanet detection, and there is value in identifying subsets of M dwarfs that are intrinsically more likely to host detectable planets Herrero et al. (2011). In particular, one might be interested in selecting stars of higher metallicity which may harbor more massive planets (Sousa et al. 2010), or young stars with relatively luminous massive planets which would be easier to detect through direct imaging (e.g. Mugrauer et al. 2010). In addition, one would like to avoid possible contaminants (e.g. background giants) or problematic systems (e.g. very active stars) from the list in order to optimize exoplanet survey efficiencies.

Determining physical properties of the (Lépine & Gaidos 2011) is also important in order to better characterize the local population of low-mass stars. This is especially true since their brightness makes them more efficient for follow-up observations and better suited to detailed study. Some of the bright M dwarfs missing from CNS3 appear to be close enough ($d \lesssim 20$ pc) to warrant inclusion in the parallax programs devoted to completing the census of low-mass stars in the Solar Neighborhood (e.g. Henry et al. 2006), in which case it is important that the candidates be first vetted through spectral typing. The Palomar-MSU spectroscopic survey Reid, Hawley, & Gizis (1995), largest of all previous spectroscopic surveys of nearby M dwarfs, provided spectral classification for 1,971 stars from the CNS3, including 1,648 stars classified as M dwarfs. Because our more recent survey is providing significant additions to bright M dwarf census over the CNS3, it is appropriate at this time to update the spectroscopic database and carry out an expanded spec-

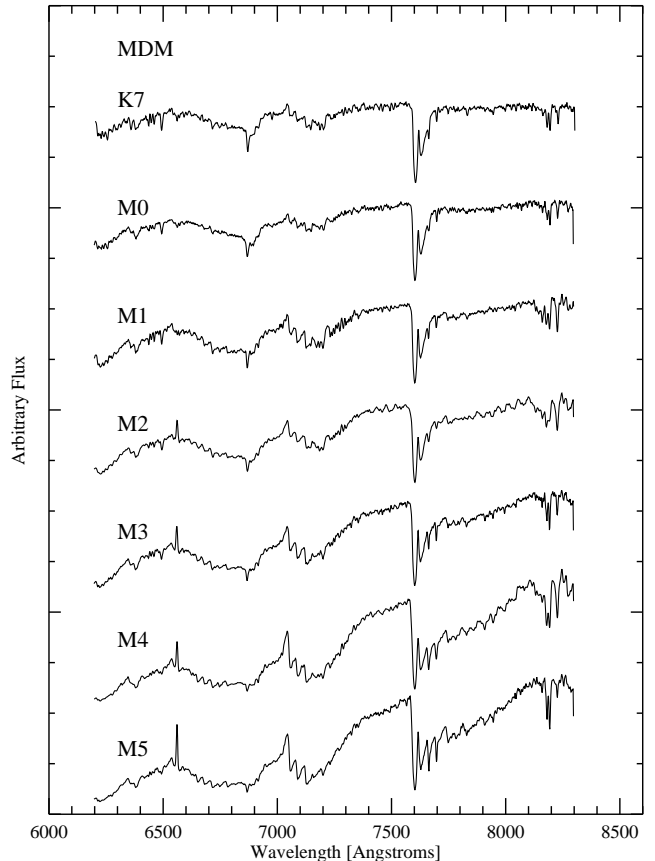


FIG. 1.— Examples of spectra collected at the MDM Observatory with either the MklIII or CCDs low-resolution spectrographs, using the McGraw-Hill 1.3-meter or Hiltner 2.4-meter telescope. All spectra covered the 6,200Å–8,700Å wavelength range with a resolution of 1.8Å–2.4Å per pixel, and a signal-to-noise ratio $20 < S/N < 30$.

troscopic survey of bright M dwarfs.

We are now conducting a spectroscopic follow-up survey of the bright M dwarf candidates identified in (Lépine & Gaidos 2011). Our goal is to provide a uniform catalog of spectroscopic measurements to initiate detailed studies of those M dwarfs and their physical properties, as well as the tailoring of exoplanet searches. In this paper, we present the first results of our survey, which provides data for the 1,556 brightest M dwarf candidates north of the celestial equator, with apparent near-infrared magnitudes $J < 9$. Observations are described in §2. Our spectral classification techniques are described in §3, and our model fitting and effective temperature determinations are given in §4. Metallicity measurements are presented in §5. Activity diagnostics are presented and analyzed in §6. A kinematic study informed by our metallicity and activity measurements is presented in §7, followed by discussion and conclusions in §8.

2. SPECTROSCOPIC OBSERVATIONS

2.1. Target selection

Stars for the follow-up spectroscopic program were selected from the catalog of 8,889 bright M dwarfs of Lépine & Gaidos (2011). The stars are identified as M dwarfs based of various color and reduced proper motions cuts. All the stars are selected to have optical-to-infrared colors $V - J > 2.7$, and have proper motions $\mu > 40$ mas yr $^{-1}$. The low proper motion limit, which eliminates nearly all background giants,

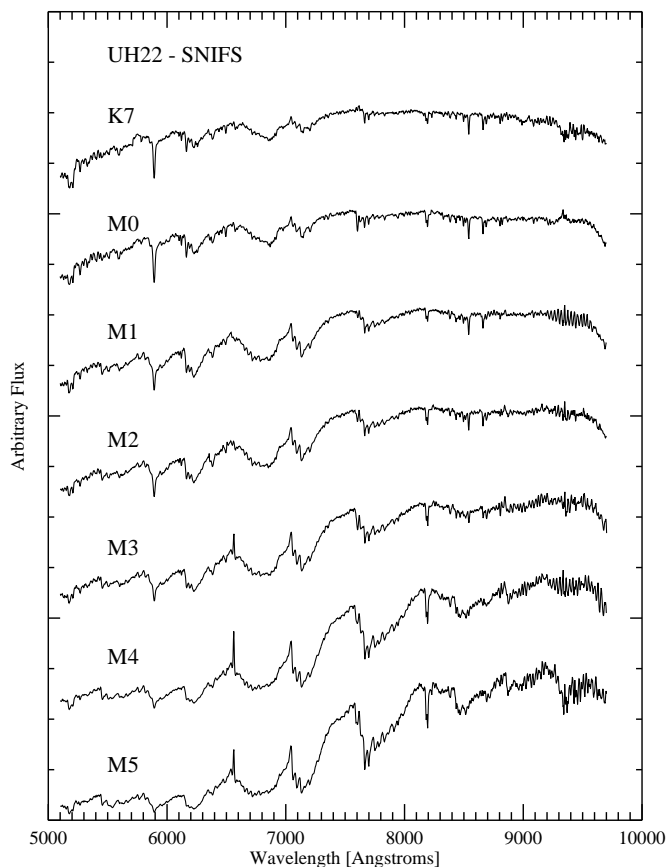


FIG. 2.— Examples of spectra collected at the University of Hawaii 2.2-meter telescope with the SNIFS spectrograph. Observations covered the 5,200Å–9,800Å wavelength regime with a spectra resolution $R \approx 2000$, and a signal-to-noise ratio $40 < S/N < 50$.

also results in a kinematic bias, which overlooks nearby bright M dwarfs with small components of motion in the plane of the sky – either due to low motion relative to the Sun or to projection effects. This kinematic bias is however relatively modest because bright M dwarfs are generally close to the Sun and tend to have large proper motions. The census for the northern sky is estimated to be $\approx 90\%$ complete.

While astrometric and photometric data have been compiled for all the stars, most lack formal spectral classification. Spectral subtypes have been estimated in Lépine & Gaidos (2011) based on a calibrated relationship between M subtype and $V-J$ color, but since the V magnitudes of many stars in the catalog are based on photographic measurements (from POSS-II plates), these colors have relatively low accuracy, and are sometimes unreliable. The relatively unreliable colors can also cause contamination of our catalog by a number of more massive G and K dwarfs, which would have otherwise failed the color cut. We have thus initiated a program of systematic spectroscopic follow-up, to provide reliable spectral typing, filter out G/K dwarfs or any remaining M giant contaminants, detect signs of chromospheric activity, and provide metallicity estimates.

A subsample of the M dwarfs with apparent infrared magnitude $J < 9$, and declinations north of the celestial equator, was assembled for the first phase of this survey. The list contains a total of 1,564 stars. We did not separate stars with well-documented spectroscopic properties from stars with no known spectroscopic data; all the stars were ob-

served indiscriminately to ensure completeness and uniformity, and allow comparison of our sample with previous studies, and in particular with the Palomar-MSU survey. Our target list also includes M dwarf spectral classification standards from Kirkpatrick, Henry, & McCarthy (1991) which we re-observed as well to provide a solid reference for our spectral classification.

Of the 1,564 M dwarf candidates, we found 286 that had been observed at the MDM observatory by one of us (SL) prior to November 2008, as part of a separate spectroscopic follow-up survey of very nearby ($d < 20$ pc) stars (Alpert & Lépine 2011). The remaining targets were distributed between our observing teams at the MDM Observatory (hereafter MDM) and University of Hawaii 2.2-meter Telescope (hereafter UH), with the MDM team in charge of higher declination targets ($\delta > 30$) and the UH team in charge of the lower declination range ($0 < \delta < 30$). In the end we obtained spectra for 1,556 stars from the initial list, nearing 99.5% completion.

To check for any possible systematic differences arising from using different telescopes and instruments, we observed 146 stars at both MDM and UH. We call this subset the “inter-observatory subset”. Observations were obtained at different times at the two observatories. Data were processed in the same manner as the rest of the sample.

The full list of observed stars, denoted by the standard SUPERBLINK catalog designations, is presented in Table 1. We also include the more widely used designations (GJ, Gl, and Wo numbers) for the 679 stars listed in the CNS3 (Gliese & Jahreiss 1991); those are often well-known objects, with abundant data from the literature. Most of the other stars (non-CNS3), however, are relatively new, and little data exists about them. Table 1 lists the sky coordinates and proper motion vectors, and parallaxes when available. The table also lists ROSAT source counts from the ROSAT all-sky points source catalogs (Voges et al. 1999, 2000), far-UV (*FUV*) and near-UV (*NUV*) magnitudes from counterpart of the stars in the GALEX fifth data release, optical V magnitude from the SUPERBLINK catalog (Lépine & Shara 2005), and infrared J , H , and K_s magnitudes from 2MASS (Cutri et al. 2003). More details on how those data were compiled can be found in Lépine & Gaidos (2011).

The optical (V band) magnitudes listed in Table 1 come from two sources with different levels of accuracy and reliability. For 911 stars in Table 1, generally the brightest ones, the V magnitude come from the Hipparcos and Tycho-2 catalogs. These are generally reliable with typical errors smaller than ± 0.1 magnitude; those stars are flagged “T” in Table 1. The 645 remaining objects have their V magnitudes estimated from POSS-I and/or POSS-II photographic magnitudes as prescribed in Lépine (2005). Photographic magnitudes of relatively bright stars often suffer from large errors at the ~ 0.5 magnitude level or more; those stars are labeled “P” in Table 1.

2.2. Observations

Spectra were collected at the MDM observatory in a series of 22 observing runs scheduled between June, 2002 and April, 2012. Most of the spectra were collected at the McGraw-Hill 1.3-meter telescope, but a number were obtained at the neighboring Hiltner 2.4-meter telescope. Two different spectrographs were used: the MkIII spectrograph, and the CCDS spectrograph. Both are facility instruments which provide low- to medium-resolution spectroscopy in the optical regime.

TABLE 1
SURVEY STARS: POSITIONS AND PHOTOMETRY.

Star name	CNS3 ^a	R.A.(ICRS) (ICRS)	Decl.(ICRS) (ICRS)	$\mu_{R.A.}$ '' yr ⁻¹	$\mu_{Decl.}$ '' yr ⁻¹	Xray ^b cnts/s	hr1 ^b	FUV ^c mag	NUV ^c mag	V mag	V flag	J ^d mag	H ^d mag	K _s ^d mag
PM I00006+1829		0.163528	18.488850	0.335	0.195				20.04	11.28	T	8.44	7.79	7.64
PM I00012+1358S		0.303578	13.972055	0.025	0.144				19.85	11.12	T	8.36	7.71	7.53
PM I00033+0441		0.829182	4.686940	-0.024	-0.085				21.18	12.04	T	8.83	8.18	7.98
PM I00051+4547	G1 2	1.295195	45.786587	0.870	-0.151					9.95	T	6.70	6.10	5.85
PM I00051+7406		1.275512	74.105217	0.035	-0.023					10.63	T	7.75	7.15	6.97
PM I00077+6022		1.927582	60.381760	0.340	-0.027	0.1700	-0.41			14.26	P	8.91	8.33	8.05
PM I00078+6736		1.961682	67.607124	-0.045	-0.091					12.18	P	8.35	7.72	7.51
PM I00081+4757		2.026727	47.950695	-0.119	0.003	0.2190	-0.27	19.68	18.91	12.70	P	8.52	8.00	7.68
PM I00084+1725	GJ 3008	2.113679	17.424309	-0.093	-0.064				19.24	10.73	T	7.81	7.16	6.98
PM I00088+2050	GJ 3010	2.224675	20.840403	-0.065	-0.247	0.0899	-0.28	21.07	16.71	13.90	P	8.87	8.26	8.01
PM I00110+0512		2.769255	5.208822	0.241	0.061			22.85	20.58	11.55	T	8.53	7.88	7.69
PM I00113+5837		2.841032	58.617561	0.056	0.029					11.21	T	8.02	7.31	7.13
PM I00118+2259		2.970996	22.984573	0.142	-0.221	0.4110	0.28		22.37	13.09	P	8.86	8.31	7.99
PM I00125+2142En		3.139604	21.713478	0.189	-0.290					11.67	T	8.84	8.28	8.04
PM I00131+7023		3.298130	70.398003	0.045	0.139				19.93	11.37	T	8.26	7.59	7.39

^a Designation in the Third Catalog of Nearby Stars (Gliese & Jahreiss 1991)

^b X-ray flux and hardness ratio from the ROSAT all-sky points source catalog (Voges et al. 1999, 2000).

^c Far-UV and near-UV magnitudes in the GALEX fifth data release.

^d Infrared magnitudes from the Two Micron All-Sky Survey ().

TABLE 2
DEFINITION OF SPECTRAL INDICES.

Index	Numerator	Denominator	Reference
CaH2	6814-6846	7042-7046	Reid, Hawley, & Gizis (1995)
CaH3	6960-6990	7042-7046	Reid, Hawley, & Gizis (1995)
TiO5	7126-7135	7042-7046	Reid, Hawley, & Gizis (1995)
VO1	7430-7470	7550-7570	Hawley et al. (2002)
TiO6	7550-7570	7745-7765	(Lépine, Rich, & Shara 2003)
VO2	7920-7960	8130-8150	(Lépine, Rich, & Shara 2003)

Their operation at either 1.3-meter or 2.4-meter telescopes is identical. Data were collected in slit spectroscopy mode, with an effective slit width of 1.0'' to 1.5''. The MkIII spectrograph was used with two different gratings: the 300 l/mm grating blazed at 8000Å, providing a spectral resolution $R \simeq 2000$, and the 600 l/mm grating blazed at 5800Å, which provides $R \simeq 4000$. The two gratings were used with either one of two thick-chip CCD cameras (*Wilbur* and *Nellie*) both having negligible fringing in the red. Internal flats were used to calibrate the CCD response. Arc lamp spectra of Ne, Ar, and Xe provided wavelength calibration, and were obtained for every pointing of the telescope to account for flexure in the system. The spectrophotometric standard stars Feige 110, Feige 66, and Feige 34 (Oke et al. 1991) were observed on a regular basis to provide spectrophotometric calibration. Integration times varied depending on seeing, telescope aperture, and target brightness, but were typically in the 30 seconds to 300 seconds range. Between 25 and 55 stars were observed on a typical night. Spectra for a total of 901 bright M dwarf targets were collected at MDM.

Additional spectra were obtained with the SuperNova Integral Field Spectrograph (SNIFS; Lantz et al. 2004) on the University of Hawaii 2.2 m telescope on Mauna Kea between February, 2009 and April, 2012. SNIFS has separate but overlapping blue (3200-5600Å) and red (5200-10000Å) spectrograph channels, along with an imaging channel, mounted behind a common shutter. The spectral resolution is ~ 1000 in the blue channel, and ~ 1300 in the red channel; the spatial resolution of the 225-lenslet array is 0.4 arc-seconds. SNIFS operates in a semi-automated mode, acquiring acquisition images to center the target on the lenslet array, and bias images

and calibration lamp spectra before and after each target spectrum. Both twilight and dome flats were also obtained each night. Integration times depended on J magnitude and were 54 s for $J = 9$. Up to 75 target spectra were obtained in one night. Spectra for 655 bright M dwarf targets were collected at UH with SNIFS.

Spectroscopic data and results are summarized in Table 3. SUPERBLINK names are given in the first column, while the second and third columns list the observatory and Julian date of the observations. The various spectroscopic measurements whose values are listed in Table 3 are described in detail in the sections below.

2.3. Reduction

2.3.1. MDM data

Spectral reduction of the MDM spectra was performed using the CCDPROC and DOSLIT packages in IRAF. Reduction included bias and flatfield correction, removal of the sky background, aperture extraction, and wavelength calibration. The spectra were also extinction-corrected and flux-calibrated based on the measurements obtained from the spectrophotometric standards. We did not attempt to remove telluric absorption lines from the spectra. Many spectra were collected on humid nights or with light cirrus cover, which resulted in variable telluric features. However, telluric features generally do not affect standard spectral classification or the measurement of spectral band indices, since all the spectral indices and main classification features avoid regions with telluric absorption.

A more common problem at the MDM observatory was slit loss from atmospheric differential refraction. Although this problem could have been avoided by the use of a wider slit, the resulting loss of the spectral resolution was deemed more detrimental to our science goals. Instead, stars were observed as close to the meridian as observational constraints allowed. In some cases, stars were observed up to ± 2 hours from the meridian however, resulting in noticeable losses. Fluctuations in the seeing, often exceeding the slit width, played a role as well. As a result, the spectrophotometric calibration was not always reliable, since the standards were only observed once per night to optimize survey efficiency. Flux recalibra-

TABLE 3
SURVEY STARS: SPECTROSCOPIC DATA

Star name	Observatory	Julian Date 2,450,000+	CaH2 _c ^a	CaH3 _c	TiO5 _c	VO1 _c	TiO6 _c	VO2 _c	Sp.Ty. ^b index	Sp.Ty. adopted	ζ	log g ^d	T_{eff} ^d K
PM I00006+1829	MDM	4791.75	G/K
PM I00012+1358S	UH22	5791.05	0.706	0.864	0.788	0.967	0.944	0.970	0.14	M0.0	1.08	5.0	3790
PM I00033+0441	UH22	5791.05	0.580	0.797	0.679	0.959	0.888	0.939	1.38	M1.5	0.93	4.5	3510
PM I00051+4547	MDM	5095.80	0.603	0.824	0.664	0.956	0.911	1.014	1.10	M1.0	1.10	4.5	3560
PM I00051+7406	MDM	5812.87	G/K
PM I00077+6022	MDM	5838.82	0.364	0.620	0.392	0.905	0.630	0.798	4.60	M4.5	0.90	5.0	3140
PM I00078+6736	MDM	5099.83	0.534	0.789	0.623	0.905	0.806	0.929	2.03	M2.0	0.96	5.0	3500
PM I00081+4757	MDM	5098.84	0.410	0.700	0.420	0.871	0.684	0.814	3.80	M4.0	1.01	5.0	3280
PM I00084+1725	UH22	5791.06	0.671	0.842	0.785	0.970	0.947	0.970	0.34	M0.5	0.91	4.5	3600
PM I00088+2050	MDM	4413.72	0.372	0.646	0.356	0.893	0.602	0.793	4.58	M4.5	0.99	5.0	3130
PM I00110+0512	UH22	5050.03	0.653	0.839	0.706	0.962	0.893	0.925	0.86	M1.0	1.16	4.5	3660
PM I00113+5837	MDM	5811.90	G/K
PM I00118+2259	UH22	5050.03	0.439	0.729	0.424	0.923	0.694	0.798	3.50	M3.5	1.10	4.5	3260
PM I00125+2142En	UH22	5791.06	0.721	0.865	0.851	0.973	0.967	0.988	-0.18	M0.0	0.80	4.5	3690
PM I00131+7023	MDM	5812.89	0.643	0.816	0.754	0.973	0.883	1.038	0.93	M1.0	0.88	4.5	3570

^a All spectral indices are corrected for instrumental effects, see Section 3.2.

^b Numerical spectral subtype M evaluated from the corrected spectral band indices (not-rounded).

^c H α spectral index, comparable to equivalent width.

^d Gravity and effective temperature from PHOENIX model fits.

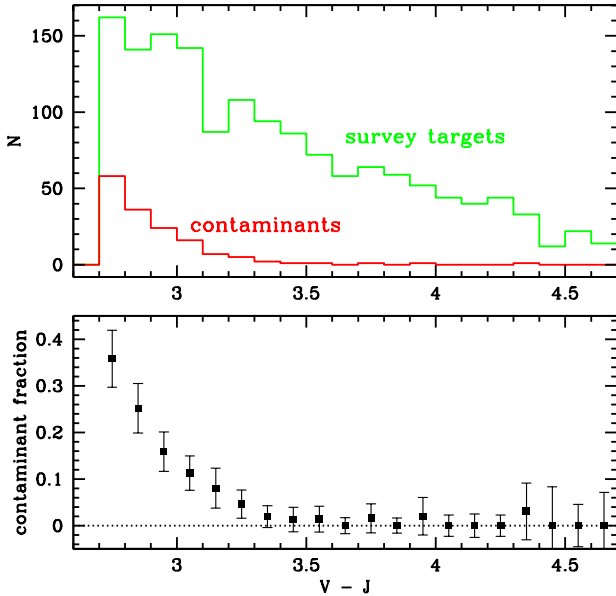


FIG. 3.— Histogram of the $V-J$ color distribution of survey stars with spectral morphologies inconsistent with red dwarf of subtype K5 and later (in red). The distribution of $V-J$ colors from the full sample is shown in green. The non-red dwarf stars are close to the blue edge of the survey, which indicates that they are most probably contaminants of the color-magnitude selection, and not the result of mis-acquisition at the telescope.

tion was therefore performed using the following procedure. Spectral indices were measured and the spectra were classified using the classification method outlined below (§3.1). The spectra were then compared to classification templates assembled from SDSS spectra. Each spectrum was divided by the classification template of the same alleged spectral subtype. In many cases, the quotients yielded a flat function, indicating that the spectrophotometric calibration was acceptable. Other quotients yielded residuals consistent with first or second order polynomials spanning the entire wavelength range, indicating problems in the spectrophotometric calibration. A second-order polynomial was fit through the quotient spectra, and the original spectrum was normalized by

this fit, correcting for calibration errors. Spectral indices were then measured again, and the spectra reclassified; this yielded changes by 0.5 to 1.0 subtypes for $\approx 20\%$ of the stars. The re-normalization was then performed again using the revised spectral subtypes. The procedure was repeated until convergence for all stars.

Finally, all the spectra were shifted in wavelength to the rest frames of their emitting stars. This was done by cross-correlating each spectrum with the SDSS template of the corresponding spectral subtype. Spectral indices were again re-measured, and the stars re-classified. Any change in the spectral subtype prompted a repeat of the flux-recalibration procedure outlined above, and the cross-correlation procedure was repeated using the revised spectral template.

A sequence of MDM spectra is displayed in Figure 1, which shows the wavelength regime and typical quality. Note the telluric absorption features near 6,850Å, 7,600Å, and 8,200Å. Signal-to-noise ratio is generally in the $30 < S/N < 50$ range near 7500Å.

2.3.2. SNIFS data

SNIFS data processing was performed with the SNIFS data reduction pipeline, which is described in detail in Bacon et al. (2001) and Aldering et al. (2006). After standard CCD pre-processing (dark, bias, and flat-field corrections), data were assembled into red and blue 3D data cubes. The data cubes were cleaned for cosmic rays and bad pixels, wavelength-calibrated using arc lamp exposures acquired immediately after the science exposures, and spectropatially flat-fielded, using continuum lamp exposures obtained during the same night. The data cubes were then sky subtracted, and the 1D spectra were extracted using a semi-analytic PSF model. We applied corrections to the 1D spectra for instrument response, airmass, and telluric lines based on observations of the Feige 66, Feige 110, BD+284211, or BD+174708 standard stars (Oke et al. 1991).

Because the SNIFS spectra are from an integral field spectrograph, operating without a slit, their spectrophotometry is significantly more reliable than the slit-spectra obtained at MDM. In fact, it is possible to perform synthetic photometry by convolving with the proper filter response.

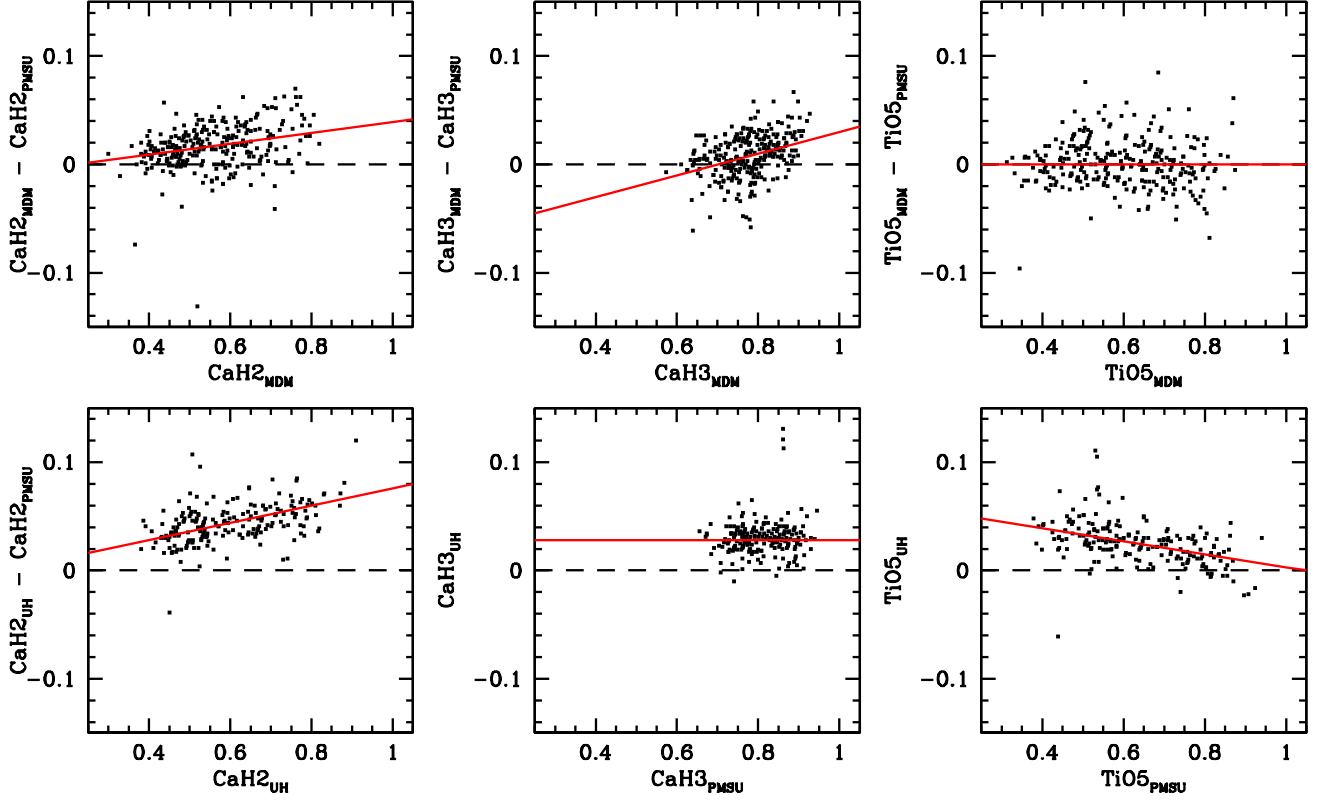


FIG. 4.— Comparison between our spectral band index measurements for a subset of 484 stars observed at MDM and UH, and the band index measurements for the same stars as reported in the Palomar-MSU spectroscopic survey of Reid, Hawley, & Gizis (1995). Small but systematic offsets are observed, which are explained by differences in spectral resolution and spectrophotometric calibration between the different observatories. These offsets demonstrate that spectral index are instrument-dependent, but that the measurements can be corrected by re-observing large subsets of stars observed elsewhere. The red segments show the fits to the offsets, which are used to determine corrections for each observatory, using the Palomar-MSU measurements as the standard.

As with the MDM data, SNIFS spectra were shifted to the rest frames of their emitting stars, by cross-correlation to SDSS templates (Bochanski et al. 2007) of the corresponding spectral subtype. Spectral indices were re-measured and the stars re-classified. This process was repeated if there was a change in the spectral subtype determination.

A sequence of UH SNIFS spectra are displayed in Figure 2, which show the wavelength range and typical data quality. Signal-to-noise ratio is generally $S/N \approx 100$ near 7500\AA .

3. SPECTRAL CLASSIFICATION

3.1. Contaminants

We first examined all the spectra by eye to identify morphological features consistent with red dwarfs of spectral subtype K5 and later. The main diagnostic was the detection of a CaH and/or TiO molecular band near 7000\AA . Of the 1556 stars observed, 1403 were found to have evidence of CaH and TiO molecular band absorption. The remaining 153 stars do not show those molecular features and must therefore be contaminants in the photometric selection.

Most of the contaminants appear to be early- to mid-type K dwarfs, and a few could be G dwarfs affected by reddening. A number of stars also displayed carbon features consistent with low gravity objects, and are possibly K giants. We suspect that many of the G and K dwarfs have inaccurate V-band magnitudes, which would make them appear to be redder than they really are, and would explain their inclusion in our color-selected sample. Other stars appear to be F/G dwarfs with

some levels of interstellar reddening, which would also explain their selection as candidate M dwarfs. Alternatively, it is possible that a number of stars were mis-acquired in the course of the survey. The very large proper motion of the sources sometimes makes them difficult to identify at the telescope, as they often have moved significantly from their positions on finder charts. Stars in crowded field are particularly susceptible to this effect. We evaluate the likelihood of those possibilities by comparing the $V-J$ color distribution of the contaminants to the distribution of the full survey sample (Figure 3, top panel); the fraction of contaminant stars in each color bin is also shown (bottom panel). The contaminants are clearly drawn from a different distribution than the full sample, and their fraction quickly drops as $V-J$ increases. If the contaminants were the result of mis-acquisition, one would expect the two distributions to be equivalent. Rather our analysis indicates that the majority of the contaminants must have been properly acquired and are simply moderately red FGK stars that slipped into the sample in the photometric/proper motion selection.

Overall we find a contamination rate of $\approx 10\%$ in our survey, although most of the contamination occurs among stars with relatively blue colors. The contamination rate is $\approx 26\%$ for red dwarf candidates in the $2.7 < V-J < 3.0$ color range. This rate drops to $\approx 8\%$ for candidates with $3.0 < V-J < 3.3$, and becomes negligible ($< 1\%$) in the redder

$$V-J > 3.3$$

candidates. The 153 stars identified as contaminants are in-

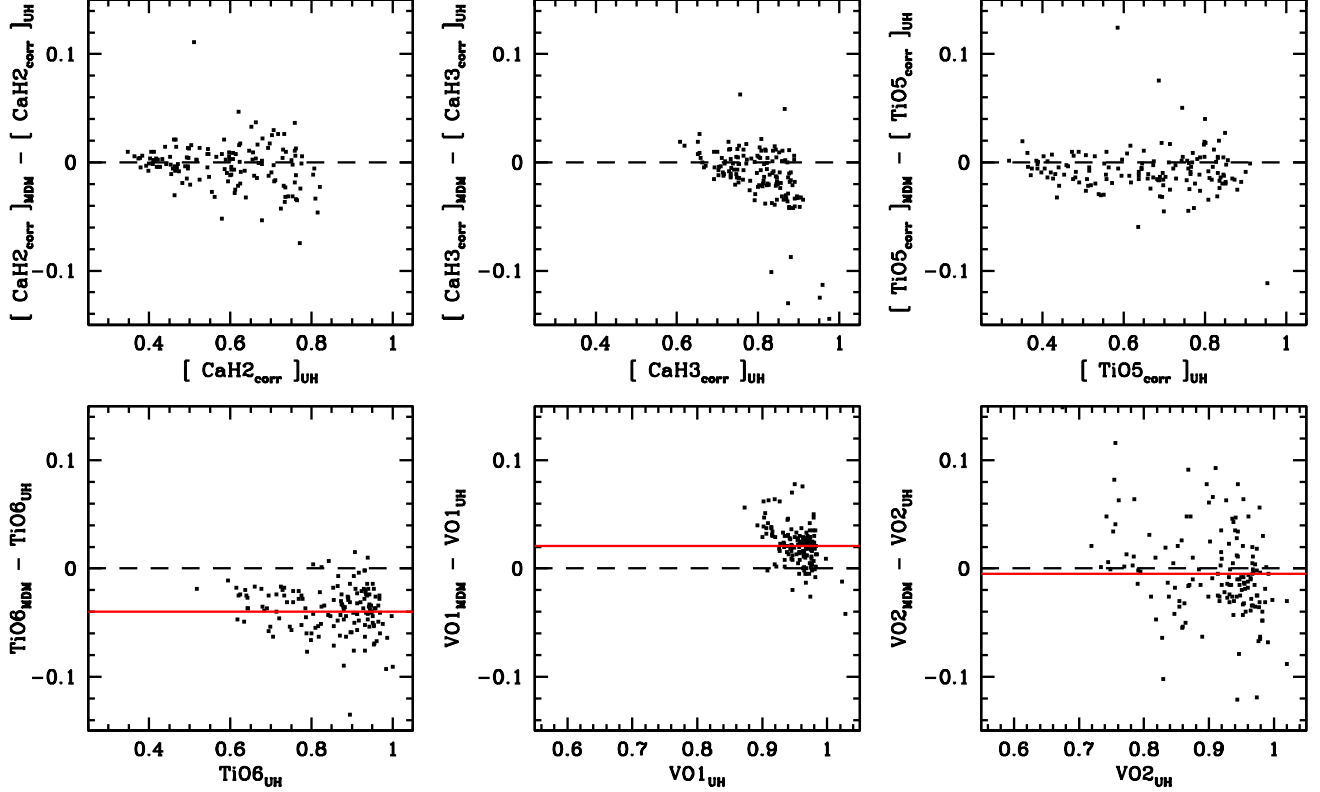


FIG. 5.— Comparison between the spectral band index measurements from MDM and the band index measurements of the same stars observed from UH. Observatory-specific corrections to the CaH2, CaH3, and TiO5 indices (see Figure 4) bring the MDM and UH values in close agreement. Small offsets are however observed for the TiO6, VO1, and VO2 indices, which we could not calibrate against Palomar-MSU survey stars. The horizontal red lines show the adopted offsets which are used to correct the MDM values to bring them in line with the UH ones. Offsets are again believed to be due to inter-observatory differences in the spectral resolution and spectrophotometric calibration.

cluded in Table 1 and Table 1 for completeness and future verification. Spectroscopic measurements such as band indices, subtypes, and effective temperature estimates are however left blank.

3.2. Classification by spectral band indices

3.2.1. Definition and measurement of band indices

To classify the stars identified as probable late-K and M dwarfs, we perform spectral classification by measuring the strength of TiO and CaH bandheads. Similar band index measurements were collected in the Palomar-MSU spectroscopic survey, and used for spectral classification. In our analysis, we use a set of four spectral band indices described in Lépine, Rich, & Shara (2003) which measure the strength of the most prominent bands of CaH, TiO, and VO in the $6000 < \lambda < 8500$ regime. The spectral indices and are listed in Table 2 along with their definition. The CaH2, CaH3, and TiO5 indices are the same as those used in the Palomar-MSU survey. The TiO6, VO1, and VO2 indices were introduced by Lépine, Rich, & Shara (2003) to better classify late-type M dwarfs, whose CaH2 and TiO5 indices become saturated at cooler tempratuers and are not as effective for accurate spectral classification of late-type M dwarfs. Each spectral band index is calculated as the ratio of the flux in the spectral region of interest (numerator) to the flux in the reference region (denominator), i.e.:

$$IDX = \frac{\int_{num} I(\lambda) d\lambda}{\int_{denom} I(\lambda) d\lambda} \quad (1)$$

Because the wavelength range for some indices is relatively narrow (especially the denominator for CaH2, CaH3, and TiO5) it is important that the spectra in which they are measured have their wavelengths calibrated in the rest frame of the star, which is why special care was made to correct all spectra for redshift/blueshift (see above).

Because molecular bandheads are relatively sharp and the spectral indices defined over relatively narrow spectral ranges, their value is also potentially dependent on spectral resolution, and may thus depend on the specific instrumental setup. In addition, the indices may be affected by systematic errors in the spectrophotometric flux calibration. One way to verify these effects is to compare index measurements of the same stars obtained at different observatories. Because of the significant overlap with the Palomar-MSU survey, we can use those stars as reference sample, and recalibrate the spectral indices so that they are consistent to those reported in Reid, Hawley, & Gizis (1995).

We identify 206 stars observed at MDM and 278 stars observed at UH which have spectral index measurements reported in the PMSU survey. The differences between our measured CaH2, CaH3, and TiO5 and thopse reported in the PSMU are plotted in Figure 4. We observe systematic trends and offsets which confirm the existence of systematic errors due to differences in resolution and flux calibration. The trends and offsets are different for the MDM and UH spectra; lower offsets are observed with the UH spectra which is consistent with the fact that the PSMU and UH spectra are similar in quality, while the MDM spectra have a higher spec-

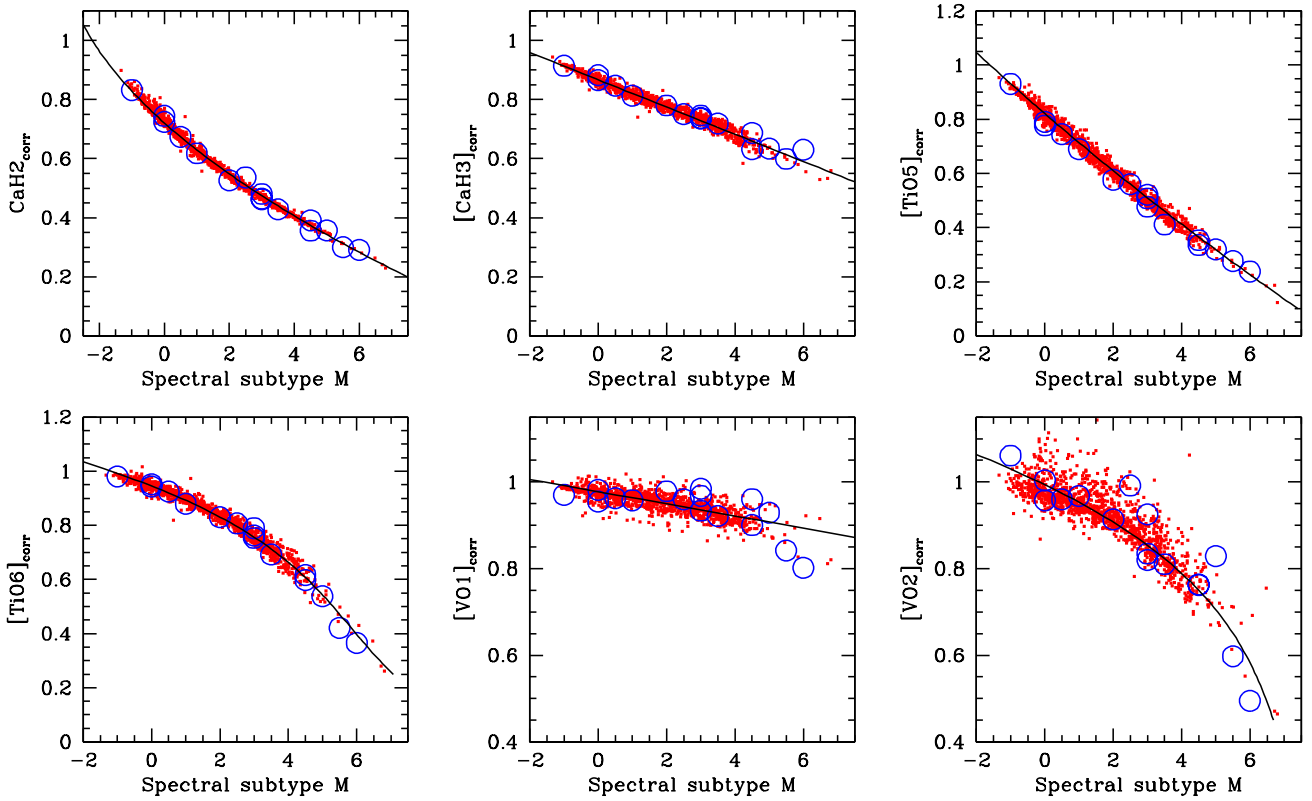


FIG. 6. — Variation of the corrected spectral indices as a function of the adopted spectral subtypes. The thin black lines show the adopted, revised calibrations for spectral classification. Blue circles show the location of a subset of classification standards from Kirkpatrick, Henry, & McCarthy (1991), which were observed in our survey; the X-axis values of those data points are the formal spectral subtypes adopted in Kirkpatrick, Henry, & McCarthy (1991), while the Y-axis values are the spectral index measurements from our survey. For our own spectral typing scheme, we calculate the average of the subtype values for the CaH2_c , CaH3_c , TiO5_c , and TiO6_c indices given by the adopted relationships. The two VO indices have relatively weak leverage on early type stars due to the shallow slope in the relationships, and are not used for assigning spectral subtypes of our (mostly early-type) survey stars.

tral resolution. We verified resolution effects by convolving the MDM spectra with a box kernel 5-pixel wide, and found that the MDM indices for the smoothed spectra had their offsets reduced by 0.01-0.02 units, bringing them more in line with the PMSU indices.

To achieve consistency in the measurements obtained at different observatories, we adopt the values from the PMSU survey as a standard of reference, and calculate corrections to the measurements from MDM and UH by fitting linear relationships to the residuals. A corrections to a spectral band index is thus applied following the general relationship:

$$IDX_c = A_{IDX:OBS} IDX_{OBS} + B_{IDX:OBS} \quad (2)$$

where IDX_{OBS} represents the measured value of an index at the observatory OBS , and $(A_{IDX:OBS}, B_{IDX:OBS})$ are the coefficients of the transformation from the observed value to the corrected one (IDX_c). Hence the corrected values of the indices CaH2 , CaH3 and TiO5 for measurements done at MDM are defined as:

$$\text{CaH2}_c = A_{\text{CaH2:MDM}} \text{CaH2}_{\text{MDM}} + B_{\text{CaH2:MDM}} \quad (3)$$

$$\text{CaH3}_c = A_{\text{CaH3:MDM}} \text{CaH3}_{\text{MDM}} + B_{\text{CaH3:MDM}} \quad (4)$$

$$\text{TiO5}_c = A_{\text{TiO5:MDM}} \text{TiO5}_{\text{MDM}} + B_{\text{TiO5:MDM}} \quad (5)$$

By definition, the measurements from the PSMU survey are used as standards for these three indices, and we have by definition $A_{\text{CaH2:PMSU}} = A_{\text{CaH3:PMSU}} = A_{\text{TiO5:PMSU}} = 1.0$, $B_{\text{CaH2:PMSU}} = B_{\text{CaH3:PMSU}} = B_{\text{TiO5:PMSU}} = 0.0$. We determine

the values of the correction coefficients from the fits to the residuals, shows as red segments in Figure 4. For $\text{OBS}=\text{MDM}$ and $\text{OBS}=\text{UH}$, the adopted correction coefficients are listed in Table 4.

To verify the consistency of the corrected spectral band index values, we compare the corrected values for the stars observed at both MDM and UH (the inter-observatory subset). The differences are shown in Figure 5. We find the corrected values CaH2_c , CaH3_c , and TiO5_c to be in good agreement, with no significant offsets beyond what is expected from measurement errors. The corrected values of all three spectral indices are listed in Table 3.

The TiO6 , VO1 , and VO2 spectral index measurements from MDM and UH are also compared in Figure 5. Those were not measured in the PMSU survey, and thus are displayed here without any correction. We find small but significant offsets between the MDM and UH values, which again point to systematic errors related to differences in spectral resolution and flux calibration. Because the UH values for CaH2 , CaH3 and TiO5 were closest to the ones from the PMSU, we adopt the UH measurements as fiducials, and determine corrections to be applied to the MDM data. The corrections are listed in Table 4 and shown as red lines in Figure 5. The corrected values of the three spectral indices are also listed in Table 3.

The scatter between the MDM and UH values, after correction, as well as the scatter between the UH/MDM and PMSU values, provide an estimate of the measurement accuracy for these indices spectral indices. Excluding a few outliers, the

TABLE 4
COEFFICIENTS OF THE SPECTRAL INDEX CORRECTIONS, BY OBSERVATORY.

<i>IDX</i>	<i>A_{IDX:PMSU}</i>	<i>B_{IDX:PMSU}</i>	<i>A_{IDX:MDM}</i>	<i>B_{IDX:MDM}</i>	<i>A_{IDX:UH}</i>	<i>B_{IDX:UH}</i>
CaH2	1.00	0.00	0.95	0.011	0.92	0.004
CaH3	1.00	0.00	0.90	0.070	1.00	-0.028
TiO5	1.00	0.00	1.00	0.000	1.06	-0.063
VO1	1.00	0.040	1.00	0.000
TiO6	1.00	-0.021	1.00	0.000
VO2	1.00	0.005	1.00	0.000

mean scatter is ≈ 0.02 units (1σ) for the CaH2, CaH3, TiO5, TiO6, and VO1 indices, and ≈ 0.04 units for VO2. This assumes that M stars do not show any significant changes in their spectral morphology over time.

3.2.2. Spectral subtype assignments for K/M dwarfs

Relationships between spectral subtype (in the M regime) and each of the spectral indices listed in Table 2 have been calibrated in (Gizis 1997) and (Lépine, Rich, & Shara 2003). Each relationship can be used to calculate a spectral subtype from one of the spectral band indices. The usual method is to combine these individual measurements, and assign a subtype based on the mean values obtained from all the spectral indices that apply. Values can then be rounded to the nearest integer or half integer. An “M subtype” with a value < 0.0 signifies that star is actually a late-K dwarf: the star is classified as K7 for an index value ≈ -1.0 and as K5 for an index value ≈ -2.0 (note: there is no K6 subtype for dwarf stars, and K7 is the subtype immediately preceding M0).

The original spectral index classification for M dwarfs/subdwarfs is largely based a relationship with the CaH2 band, which is one of the deeper bands at all spectral subtypes, and the deepest band in metal-poor M subdwarfs in the red Gizis (1997); Lépine, Rich, & Shara (2003). The original relationship is: $[SpTy]_{CaH2} = 10.71 - 20.63 CaH2 + 7.91 (CaH2)^2$. To verify this relationship, we estimated spectral subtypes from our corrected indices $CaH2_c$ for 16 spectroscopic calibration stars from Kirkpatrick, Henry, & McCarthy (1991) which were observed as part of our survey, and spanning subtypes K7.0 to M6.0. We found small but significant differences in our estimated spectral subtypes and the values formally assigned by Kirkpatrick, Henry, & McCarthy (1991); the values estimated from the Gizis (1997) relationship tend to systematically underestimate the subtypes by ≈ 0.5 units for stars later than M3. To improve on the index classification method, we performed a χ^2 polynomial to the classification standards and obtained the revised relationship:

$$[SpTy]_{CaH2} = 11.50 - 21.71 CaH2_c + 7.99 (CaH2)^2 \quad (6)$$

which corrects for the observed offsets at later types. Starting with this relationship, and guided by the formal spectral subtype from the classification standards, we performed additional χ^2 polynomial fits to calibrate additional index-subtype relationships for CaH3, TiO5, and TiO6:

$$[SpTy]_{CaH3} = 18.80 - 21.68 CaH3_c \quad (7)$$

Where the corrected values of the spectral bands indices (see Eqs.2-5) are used. The relationships are slightly different from those quoted in Gizis (1997) and Lépine, Rich, & Shara (2003) but are internally consistent to each other, whereas an

application of the older relationships to our corrected band index measurements would yield internal inconsistencies, with subtype difference up to 1 spectral subtype between the relationships.

The ratio of oxides (TiO, VO) to hydrides (CaH, CrH, FeH) in M dwarfs is known to vary significantly with metallicity (Gizis 1997; Lépine, Rich, & Shara 2007). In the metal-poor M subdwarfs, it is the oxides bands that appear to be weaker, while hydride bands remain relatively strong (in the most metal-poor ultrasubdwarfs, or usdM, the TiO bands are almost undetectable). Therefore it makes sense to rely more on the CaH band as the primary subtype/temperature calibrator. The same $[SpTy]_{CaH2}$ and $[SpTy]_{CaH3}$ relationships should be used to determine spectral subtypes at all metallicity classes (i.e. in M subdwarfs as well as in M dwarfs).

Because the TiO and VO bands are also strong in the metal-rich M dwarfs, it is still useful to include these bands as secondary indicators, to refine the spectral classification. In the late-type M dwarfs, in fact, the CaH bandheads are saturating, and one has to rely on TiO and VO bands to properly classify the stars. The main caveat in using the oxide bands for spectral classification is that this can potentially introduce a metallicity dependence on the estimated spectral subtype, with more metal-poor stars being assigned as earlier subtype than what they would based on the strength of their CaH bands alone. In any case, because our sample appears to be dominated by near-solar metallicity stars, we fit additional relationships between subtype and the TiO5 and TiO6 bands indices. We first recalculate the subtypes by averaging the values of $[SpTy]_{CaH2}$ and $[SpTy]_{CaH2}$, and a χ^2 fit yields:

$$[SpTy]_{TiO5} = 7.83 - 9.55 TiO5_c \quad (8)$$

$$[SpTy]_{TiO6} = 9.92 - 15.68 TiO6_c + 21.23 (TiO6_c)^2 - 16.65 (TiO6_c)^3 \quad (9)$$

where again the corrected band indices are used. The relatively sharp non-linear deviation in the TiO6 distribution around M3 forces the use of a third order polynomial in the fit.

We also determine the relationships for the VO1 and VO2 band indices. After recalculating the subtypes from the average of $[SpTy]_{CaH2}$ and $[SpTy]_{CaH2}$, $[SpTy]_{TiO5}$, and $[SpTy]_{TiO6}$, we find:

$$[SpTy]_{VO1} = 69.8 - 71.4 [VO1]_c \quad (10)$$

$$[SpTy]_{VO2} = 9.56 - 12.47 [VO2]_c + 22.33 ([VO2]_c)^2 - 19.59 ([VO2]_c)^3 \quad (11)$$

The VO indices however make relatively poor determinations of spectral subtypes, mainly because the shallower slope at

earlier subtypes provides little leverage. The VO2 index also shows unexpectedly large scatter in the MDM spectra, including in the classification standard stars, which we suspect is due the fact that the index is defined very close to the red edge of the MDM spectral range and more subject to statistical noise and flux calibration errors. We therefore do not include $[SpTy]_{VO12}$ and $[SpTy]_{VO2}$ in the final determination of the spectral subtypes.

Fig. 6 plots all the corrected spectral band indices as a function of the adopted spectral subtype. The relatively small scatter (≈ 0.02) in the distribution of $[CaH2]_c$, $[CaH3]_c$, $[TiO5]_c$ and $[TiO6]_c$ demonstrate the internal consistency of the spectral type calibration for the four indices. All four relationships have an average slope ≈ 10 ; since those indices have an estimated measurement accuracy of ≈ 0.02 units, we estimate that spectral subtypes calculated by combining the four indices should be accurate to about ± 0.10 subtype assuming that the measurement errors in the four indices are uncorrelated (which they may not be). In any case, we follow the general convention and assign spectral subtype to the nearest half integer. To verify the consistency of the spectral classification, we compare the spectral types evaluated independently for the list of 141 stars observed at both MDM and UH. We find that 82% of the stars have the same spectral type, i.e. spectra assigned to the same half-subtype; this suggests a 1σ error of ± 0.18 on the spectral type determination, and justifies the use of half-subtypes as the smallest unit for our classification.

The resulting classifications based on the CaH and TiO band index measurements are listed in Table 3. The method provides fractional values of the spectral types, which we list to 2 decimal figures. Given that the subtypes are really accurate to only about half a subtype, we round these values to the nearest half integer, and adopt these as the official spectral subtypes. The non-rounded values are however useful for comparison with other physical parameters as they provide a continuous range of fractional values; these are used in the analysis throughout the paper, though the subtypes should formally be quoted only to half an integer.

A histogram of the distribution of spectral subtypes is shown in Figure 7. Most of the stars in our survey have subtypes in the M0-M3 range. The sharp drop for stars of subtypes K7.5 and earlier is explained by the color selection used in the Lépine & Gaidos (2011) catalog ($V-J > 2.7$) which was originally intended to select only M dwarfs. The selection criterion appears to be efficient in selecting out K dwarfs. The distribution also shows a marked drop in numbers for subtypes M4 and later. This is a consequence of the relatively bright magnitude limit ($J < 9$) of our follow-up survey combined with the low absolute magnitudes of late-type M dwarfs, which only includes. The late-type M dwarfs targeted for our survey are selected over a small volume of stars at very close distance range from the Sun.

3.3. Semi-automated classification using THE HAMMER

To verify the accuracy and consistency of spectral typing based the spectral-index method described above, we performed independent spectral classification using the Hammer code (Covey et al. 2007). The Hammer was designed to classify stars in the Sloan Digital Sky Survey Spectroscopic database, including M dwarfs (West et al. 2011). The code works by calculating a variety of spectral-type sensitive band indices, and uses a best-fit algorithm to identify the spectral subtype providing the best fit to those band indices. For late-

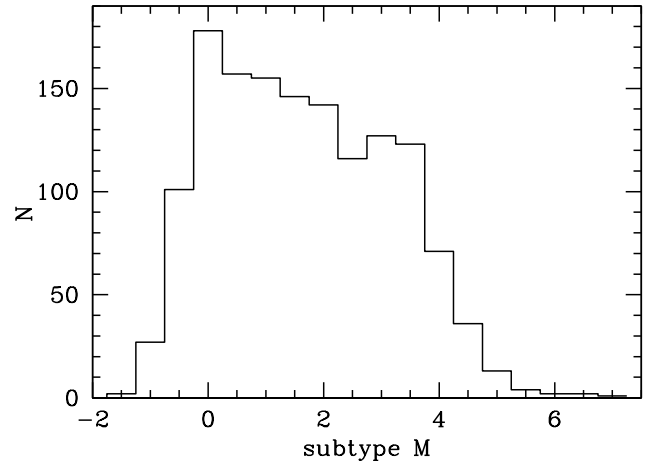


FIG. 7.— Distribution of our survey stars by spectral subtype M, with K5=-2 and K7=-1. Most of the stars in our survey are early-M objects. The sharp drop at subtypes K7.5 and earlier is a consequence of our initial $V-J > 2.7$ color cut, which was meant to select M dwarf stars only. The sharp drop for subtypes M4 and later is a consequence of the high magnitude limit ($J < 9$) of our survey, which restricts the distance range over which late-M stars are detected. The magnitude limit also explains the slop drop in numbers from M0 to M3.

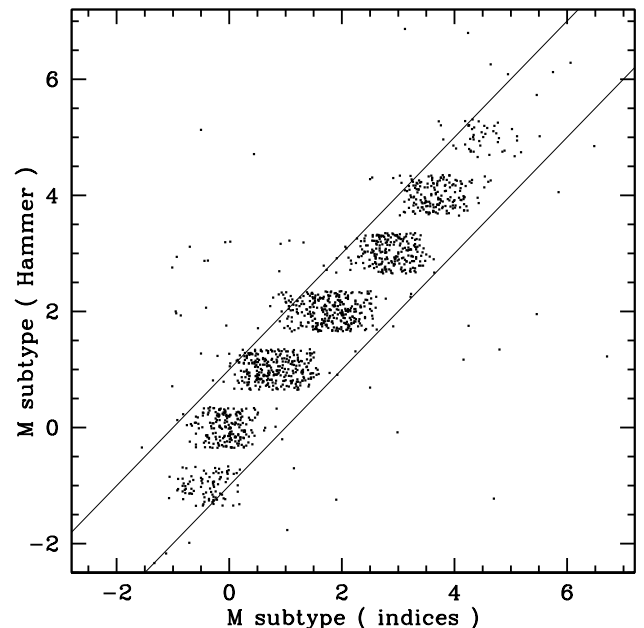


FIG. 8.— Comparison of spectral types assigned by the spectral index method and those assigned by the Hammer code, used for stellar classification in the Sloan Digital Sky Survey. Subtypes generally agree to within the advertised precision of the Hammer (± 1 subtype, illustrated by the slanted lines), although the Hammer subtypes are marginally later than the spectral index subtypes, by 0.27 subtype on average.

K and M dwarfs, spectral subtypes are determined to integer value (K5, K7, M0, M1, ..., M9).

However, to ensure that the automatically determined spectral types were accurate, we used the manual “eye check” mode of the Hammer (version 1.2.5). This mode is typically used to verify that there are no incorrectly typed interlopers. The Hammer allows the user to compare spectra to a suite of template spectra to determine the best match. West et al. (2011) have found that for late-type M dwarfs, the automatic classifications were systematically one subtype earlier than

TABLE 5
COLORS AND T_{eff} FOR RED DWARFS IN OUR SURVEY AS A
FUNCTION OF SPECTRAL SUBTYPE.

subtype	$NUV - V^1$	σ_{NUV-V}^1	$\overline{V-J}$	σ_{V-J}	$\overline{T_{eff}}$	$\sigma_{T_{eff}}$
K 7.0	8.17	0.21	2.90	0.31	4073	98
K 7.5	8.60	0.31	2.89	0.16	3883	82
M 0.0	8.66	0.36	2.94	0.21	3762	71
M 0.5	8.74	0.30	3.11	0.34	3646	48
M 1.0	8.89	0.39	3.19	0.18	3565	44
M 1.5	9.07	0.38	3.36	0.23	3564	39
M 2.0	9.25	0.47	3.52	0.34	3518	57
M 2.5	9.45	0.50	3.69	0.28	3500	61
M 3.0	9.61	0.38	3.91	0.28	3423	62
M 3.5	9.69	0.33	4.17	0.33	3320	66
M 4.0	9.72	0.35	4.45	0.41	3204	76
M 4.5	4.81	0.46	3119	43
M 5.0	5.23	0.50	3014	61

¹ Non-active (“quiescent”) red dwarfs only.

those determined visually. Our analysis confirms this offset, and we therefore disregarded the automatically determined Hammer values to adopt the visually determined subtypes.

The resulting subtypes are listed in Table 3. Some 167 stars are not found to be good fits to any of the K5, K7 or M type templates, and could be either early K or G dwarfs. Accordingly these are labeled “G/K” in Table 3. These stars are clearly neither late-K or M dwarfs, and are thus most likely early-type contaminants which made the target list due to inaccurate or unreliable $V-J$ colors.

A comparison of spectral subtypes determined from the spectra-index and Hammer methods is shown in Figure 8, top panel. Because the Hammer yields only integer subtypes, respectively, we have added random values in the $-0.4, 0.4$ range to the hammer subtypes to facilitate the comparison. Slanted lines in Figure 8 show the range expected if the classification methods are to agree to within 1.0 subtypes.

Figure 8 also reveals a number of outliers with large differences in spectral subtypes between the two methods. We found 48 stars with differences in spectral subtyping larger than ± 1.5 subtypes. The spectra from these stars were examined by eye: except for one star, we found the band-index classifications to agree much better with the spectra than the Hammer determined subtypes, as we compare the spectra to our list of classification standards. The one exception is the star PM I11055+4331 (Gl 412B) which the band index measurements classify as M 6.5, but the Hammer determined subtype of M 5.0 appears to be more accurate. This exception likely occurs because of the saturation of the CaH2 and CaH3 subtypes in the late-type star, which make the band-index classification less reliable.

3.4. Color/spectral-type relationships

Spectral subtypes were estimated in Lépine & Gaidos (2011) based on $V-J$ colors alone. Here we verify this assumption and re-evaluate the color-magnitude relationship for bright M dwarfs. The $V-J$ color index combines estimated optical magnitudes from the SUPERBLINK catalog to the 2MASS infrared J magnitudes of their counterparts. The SUPERBLINK V magnitudes are estimated either from the Tycho-2 catalog V_T magnitudes, or from a combination of the Palomar photographic B_J (IIIaJ), R_F (IIIaF), and I_N (IVn) magnitudes, as described in Lépine & Shara (2005). Values of V are more accurate for the former (≈ 0.1 mag) than for the latter ($\gtrsim 0.5$ mag); Table 1 indicates the source of the V magnitude.

The $V-J$ colors of our stars are plotted as a function of

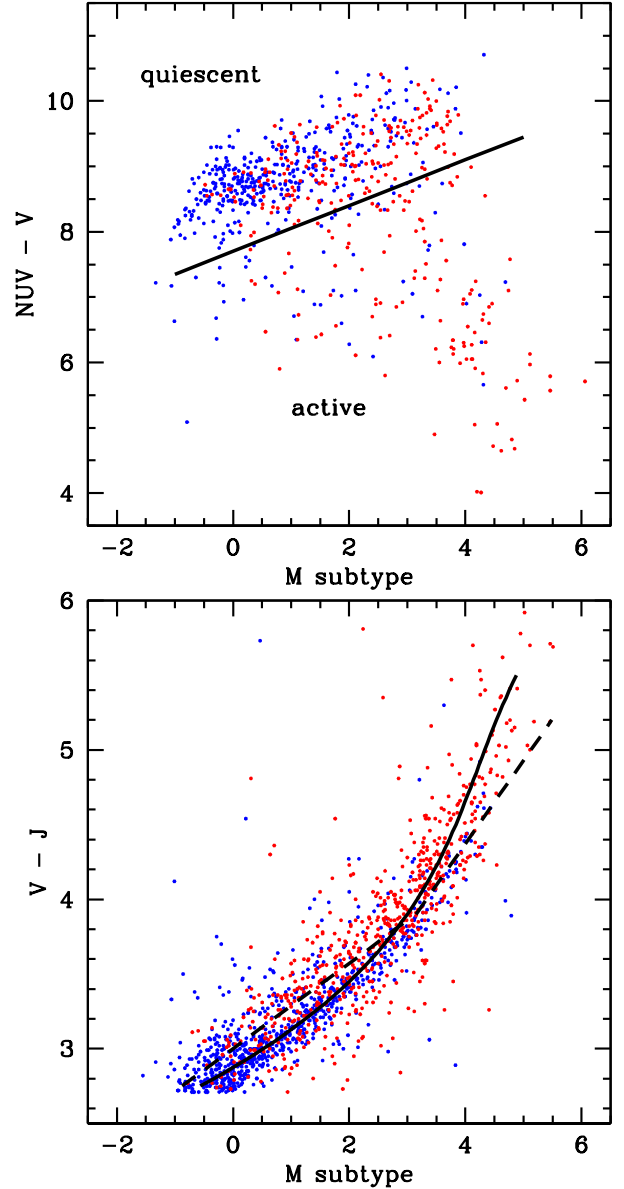


FIG. 9.— Variation of the UV-to-optical $NUV - V$ color index and the optical-to-IR $V - J$ color index as a function of spectral subtype M. Stars with more reliable V magnitudes from the Tycho-2 catalog are shown in blue, stars with V magnitudes derived from less reliable photometric measurements are shown in red. The distribution of ultra-violet to optical colors ($NUV - V$) with spectral subtype shows two populations, one with a tight correlation, consistent with blackbody distribution and labeled “quiescent”, and a scattered population of stars with clear UV excess, labeled “active”. The distribution of $V - J$ with subtype closely follows the relationship used by Lépine & Gaidos (2011) to predict subtypes from $V - J$ colors (dashed line) except for stars of later subtypes which have redder colors than predicted. A revised relationship (full line) is fitted to the data. Outliers point to stars with bad V magnitude measurements.

spectral subtype in Figure 9 (bottom panel). The adopted color-subtype relationship from Lépine & Gaidos (2011) is shown as a thick dashed line. Stars with the presumably more reliable Tycho-2 magnitudes are shown in blue, while stars with photographic V magnitudes are shown in red. Stars with Tycho-2 V magnitudes appear to have bluer colors at each spectral subtype; this however is an effect of the visual magnitude limit of the Tycho-2 catalog, which includes only the brightest stars in the V band and thus reaches the bluer ob-

jects. The Lépine & Gaidos (2011) relationship generally follows the distribution at all subtypes, but with mean offsets up to $\pm 0.4\text{mag}$ in $V-J$, especially at earlier and later subtypes. We perform a χ^2 fit to determine the following, improved relationship:

$$[\text{SpTy}]_{V-J} = -32.79 + 20.75(V-J) - 4.04(V-J)^2 + 0.275(V-J)^3 \quad (12)$$

after exclusion of $3\text{-}\sigma$ outliers. The relationship is shown in Figure 9 (solid line). There is a scatter of 0.7 subtype between $[\text{SpTy}]_{V-J}$ and the subtype determined from spectral band indices. While the spectroscopic classification is more accurate and reliable, photometrically determined spectral subtypes using the equation above are accurate to ± 0.5 subtype 80% of the time, and to ± 1.0 subtype 95% of the time, for stars in our survey.

We also compare the near-UV to optical magnitude color $NUV-V$ for the 714 stars in our sample which have counterparts on GALEX. We find that a majority of the stars display a slow increase in color as a function of subtype, from $NUV-V = 8$ at M0 to $NUV-V = 10$ at M4. There is however a significant fraction of M dwarfs which display much bluer $NUV-V$ colors at any given subtype. The excess in NUV flux is strongly suggestive of chromospheric activity (see §6 below for a more detailed analysis). We separate the active stars from the more quiescent objects with the following condition:

$$[NUV-V] > 7.7 + 0.35 [\text{Spty}] \quad (13)$$

where $[\text{Spty}]$ is the mean spectral subtype calculated from equations 8-11. After excluding active stars, we calculate the mean values and scatter about the mean of $NUV-V$ for each half-integer spectral subtype. Again those are listed in Table 5 for reference. There is not a sufficient number of stars to calculate mean values and scatter at M4.5 (1 star) and M5.0 (0 star).

4. PHOENIX MODEL FITS AND T_{EFF} ESTIMATES

We compared the spectra to a grid of 298 models of K- and M-dwarf spectra generated by the BT-SETTL version of PHOENIX (Allard et al. 2010). BT-SETTL includes updated opacities (i.e. of H_2O), revised solar abundances (Asplund et al. 2009), a refractory cloud model, and rotational hydrodynamic mixing. The models include effective temperatures T_{eff} of 3000-5000 K in steps of 100 K, $\log g$ values of 4, 4.5, and 5, and metallicities of $[\text{M}/\text{H}] = -1.5, -1, -0.5, 0, +0.3, \text{ and } +0.5$. For each temperature, $\log g$ and metallicity value, we selected the model with α/Fe that was closest to solar.

The spectral density of model calculations varies with wavelength but is everywhere vastly greater than the resolution of our spectra. Model spectra were convolved with a gaussian with FWHM of the same resolution as the spectra, and a corrective shift (typically less than a resolution element) was found by cross-correlating the observed and model spectra. Normalized spectra were ratioed and χ^2 calculated using the variance spectrum of the observations. We restricted the spectral range over which χ^2 is calculated to 5600-9000Å and exclude the problematic region 6400-6600Å which contains poorly-modeled TiO absorption (Reyle et al. 2011). We also excluded regions where the telluric correction is rapidly changing with wavelength, i.e. the slope, smoothed over 4 resolution elements or 11.7\AA , exceeds 1.37\AA^{-1} . The model

with the minimum χ^2 was identified. For a more refined estimate of effective temperature, we selected the 7 best-fit models and construct 10,000 linear combinations of them; the “effective temperature” of each is the weighted sum of the temperatures of the components. We again found the model with the minimum χ^2 . We calculated the standard deviation of T_{eff} among the combination models as a function of the maximum allowed χ^2 . We reported the maximum standard deviation as a conservative estimate of uncertainty. We also calculated formal 95% confidence intervals for T_{eff} based solely on the expected distribution of χ^2 for $N-3$ degrees of freedom, where $N \sim 1100$ is the number of resolution elements used in the fit. The parameters of the best-fit model, and the refined T_{eff} , standard deviation, and confidence intervals are reported in Table 3.

Values of T_{eff} calculated for individual stars are plotted in Figure 10 as a function of their spectral subtype (grey dots). Median values for stars within each half-subtype bin are plotted in black, with error bars showing the interquartile ranges. Our model-fit algorithm prefers values that match the T_{eff} model grid, which have a 100K grid step (i.e., 3500K is preferred over 3510K).

Our results suggest the existence of a T_{eff} plateau spanning M1-M3. To investigate this further, we compare our values to the effective temperatures reported in Casagrande, Flynn, & Bessell (2008) for 18 of the stars in our sample, and in (Rojas-Ayala et al. 2012) for another 49 stars; our own spectral type determinations are combined to the T_{eff} measured by the other authors. The values are compared in Figure 10. We find that our mid-type plateau is corroborated with the (Rojas-Ayala et al. 2012) values, but not with those from Casagrande, Flynn, & Bessell (2008), whose values decrease monotonically with spectral subtype. The effective temperatures in Casagrande, Flynn, & Bessell (2008) are based on photometric measurements, while the (Rojas-Ayala et al. 2012) values are estimated by PHOENIX model fits to infrared spectra. It is interesting that the fits to the optical and infrared spectra yield T_{eff} values which are in agreement. The disagreement with the photometric determinations however suggest that atmospheric models for M dwarfs are still not well understood, in particular in the M1-M4 spectral regimes.

5. THE ζ -PARAMETER AND METALLICITY ESTIMATES

5.1. Recalibration of the ζ parameter

The $\zeta_{\text{TiO}/\text{CaH}}$ parameter (denoted ζ for short) is a combination of the TiO5, CaH2, and CaH3 spectral indices which was shown to be correlated with metallicity in metal-poor M subdwarfs (Woolf, Lépine, & Wallerstein 2009). The index was first described in Lépine, Rich, & Shara (2007), and a revised calibration has recently been proposed by Dhital et al. (2012). The index measures the relative strength of the TiO molecular band around 7,000Å with respect to the nearby CaH molecular band. In cool stars, the ratio between TiO and CaH is a function of both gravity and metallicity. The CaH band is noticeably stronger in giants (Mann et al. 2012), and this effect can be used as effective means to separate out M giants from M dwarfs using optical spectroscopy. In the higher gravity M dwarfs/subdwarfs however, the TiO to CaH ratio is believed to be mostly affected by metallicity. TiO opacities are significantly weaker in metal-poor stars, and the strength or weakness of the TiO band relative to CaH has long been used to identify low-mass, metal-poor halo stars in the Solar Neigh-

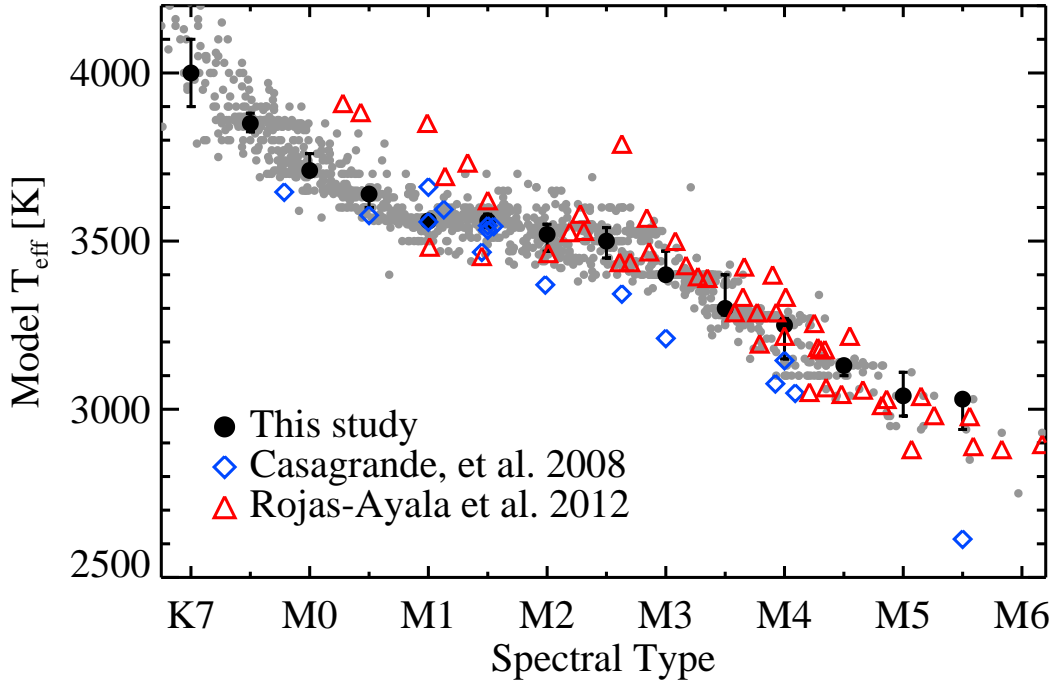


FIG. 10.— Effective temperatures for the bright M dwarfs in our survey determined by fits to the PHOENIX models. The gray points represent individual objects, while the large black points are the median values of the objects within each half subtype bin. The error bars are the interquartile ranges. Blue diamonds and red triangles show the T_{eff} estimates for subsets of stars in our survey whose temperatures were estimated from photometry Casagrande, Flynn, & Bessell (2008) and model fits to infrared spectra (Rojas-Ayala et al. 2012) respectively. While both spectroscopic estimates show evidence of a plateau at M2-M3, the photometric estimates do not concur.

borhood (Mould 1996; Gizis 1997).

The ζ parameter was originally introduced to rank metal-poor, main-sequence M stars into three metallicity classes (Lépine, Rich, & Shara 2007); stars with $0.5 < \zeta < 0.825$ are formally classified as subdwarfs (sdM), $0.2 < \zeta < 0.5$ defines extreme subdwarfs (esdM), while a $\zeta < 0.2$ identifies the star as an ultrasubdwarf (usdM). However, it is conjectured that ζ could be used to measure metallicity differences in disk M dwarfs, i.e. at the metal-rich end. Disk M dwarfs are generally found to have $0.9 < \zeta < 1.1$, though it is unclear if variation in ζ correlates with metallicity for values within that range. Measurement of Fe lines in a subset of M dwarfs and subdwarfs does confirm that the ζ parameter is correlated with metallicity (Woolf, Lépine, & Wallerstein 2009), with $\zeta \simeq 1.05$ presumably corresponding to solar abundances. However there is a significant scatter in the relationship which raises doubts about the accuracy of ζ as a metallicity diagnostic tool.

A critical point is that the TiO/CaH ratio is not sensitive to the classical iron-to-hydrogen ratio Fe/H, but rather depends on the relative abundance of α -elements to hydrogen (α/H) because both O and Ti are α -elements. Variations in α/Fe would thus weaken the correlation between ζ and Fe/H. The index also has significantly more leverage at later subtypes. This is because the strengths of both the TiO and CaH bands are generally greater, and their ratio can thus be measured with higher accuracy. The index is much less reliable at earlier M subtypes, and in particular for late-K stars.

A more important issue is the specific calibration adopted for the ζ parameter, which is a complicated function of the TiO5, CaH2, and CaH3 indices. The ζ parameter itself is

defined as:

$$\zeta = \frac{1 - \text{TiO5}}{1 - [\text{TiO5}]_{Z_{\odot}}}, \quad (14)$$

which in turns depend on $[\text{TiO5}]_{Z_{\odot}}$, which is a function of CaH2+CaH3. The function $[\text{TiO5}]_{Z_{\odot}}$ is supposed to estimate the expected value of the TiO5 index in stars of solar metallicity, for a given value of CaH2+CaH3. The original definition of the ζ index (Lépine, Rich, & Shara 2007) defined $[\text{TiO5}]_{Z_{\odot}}$ as:

$$[\text{TiO5}]_{Z_{\odot}} = -0.050 - 0.118 \text{CaH} + 0.670 \text{CaH}^2 - 0.164 \text{CaH}^3 \quad (15)$$

where $\text{CaH} = \text{CaH2} + \text{CaH3}$. The more recent calibration of Dhital et al. (2012), on the other hand, uses:

$$[\text{TiO5}]_{Z_{\odot}} = -0.047 - 0.127 \text{CaH} + 0.694 \text{CaH}^2 - 0.183 \text{CaH}^3 - 0.005 \text{CaH}^4. \quad (16)$$

The difference between the two calibrations is mainly in the treatment of late-K and early-type M dwarfs, as illustrated in Figure 11. When overlaid on the distribution of CaH2+CaH3 and TiO5 values from our current survey, however, the two calibrations fail to properly fit the distribution of data points at the earliest subtypes (high values of CaH2+CaH3 and TiO5). This will result in the Lépine, Rich, & Shara (2007) overestimating the metallicity at earlier subtypes, while the Dhital et al. (2012) calibration will underestimate it.

In any case, evidence for variations in the spectral indices due to spectral resolution and flux calibration, which

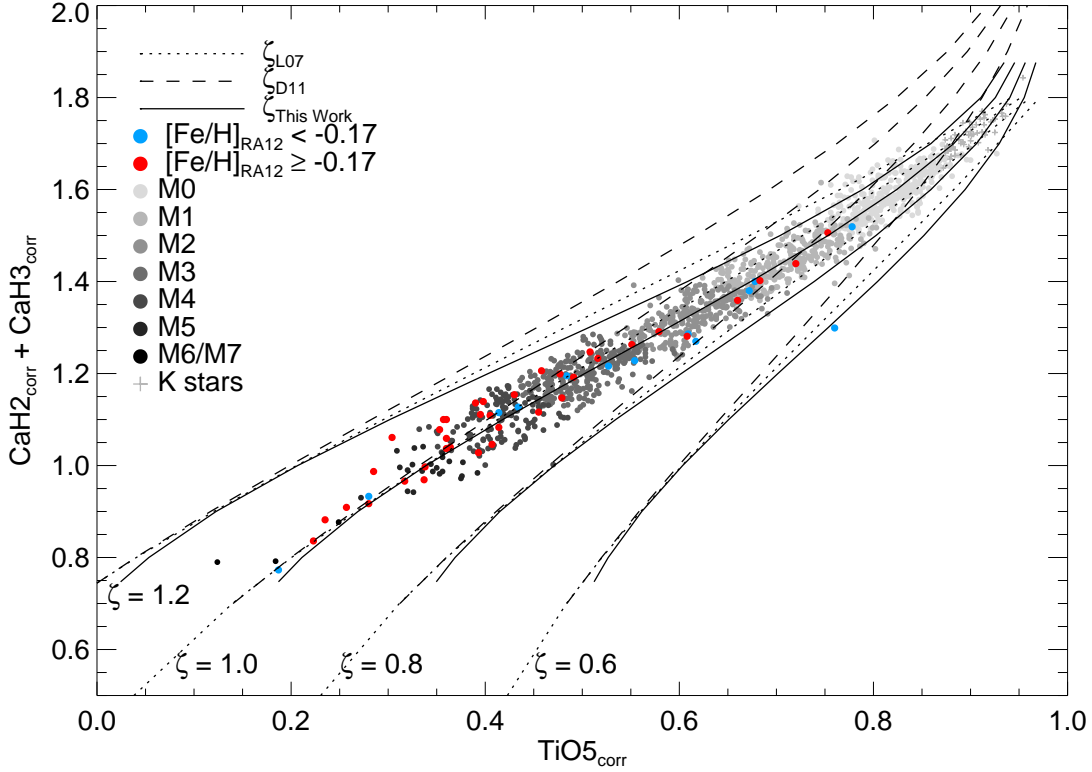


FIG. 11.— Distribution of corrected CaH2+CaH3 vs TiO5 band index values for the stars in our survey (grey dots - with brightness levels correlating with spectral subtype). There is a tight correlation between the two indices, which are both also correlated with spectral subtypes, with earlier stars on the upper right of the diagram as shown. The distribution is used as a guide to calibrate the value of ζ , with $\zeta = 1$ assumed to trace the CaH2+CaH3/TiO5 relationship for stars with average Galactic disk abundances (near-solar). The iso- ζ contours from the earlier calibrations of Lépine, Rich, & Shara (2007) and Dhital et al. (2012) are shown as dotted and dashed lines, respectively. When applied to our corrected spectral index values, they both diverge from the observed distribution at earlier subtypes, with the Lépine, Rich, & Shara (2007) overestimating the ζ of late-K and early-M dwarfs, while the Dhital et al. (2012) calibration yield underestimates. This emphasizes again the need to use properly recalibrated and corrected spectral index values (see Figures 4-5). Our revised, dataset-specific calibration is shown with the continuous lines. Known metal-rich and metal-poor stars are denoted in red and blue, respectively.

are instrument/observatory specific, indicates that the calibrations of the ζ parameter are generally valid only for specific datasets, and should only be used on data from a different observatory if the spectral index measurements yield consistent values, or after corrections have been applied as described in Section 3.2. Because we do not have any star in common with the Dhital et al. (2012) subsample, we cannot verify the consistency of their ζ calibration to our data at this time. In addition, because we have now applied a correction to our MDM spectral index measurements, the Lépine, Rich, & Shara (2007) calibration of ζ may now be off, and should not be used for our sample.

Instead, we recalibrate the ζ parameter using our corrected spectral index values. Our fit of $[\text{TiO5}]_c$ as a function of $[\text{CaH}]_c = [\text{CaH2}]_c + [\text{CaH3}]_c$ yields:

$$[\text{TiO5}]_{Z_\odot} = -0.588 + 2.211 ([\text{CaH}]_c) - 1.906 ([\text{CaH}]_c)^2 + 0.622 ([\text{CaH}]_c)^3. \quad (17)$$

We calculate the new ζ values using the corrected values of the TiO5 index, i.e.:

$$\zeta = \frac{1 - [\text{TiO5}]_c}{1 - [\text{TiO5}]_{Z_\odot}}. \quad (18)$$

All our values of ζ are listed in Table 3.

In order to evaluate the accuracy of the ζ measurements, we compared values of ζ independently measured at both MDM

and UH for the 146 stars in our inter-observatory subset. Values are compared in Figure 12 (top panel) which shows $\Delta\zeta = \zeta_{\text{MDM}} - \zeta_{\text{UH}}$ as a function of spectral subtype. We find a mean offset $\Delta\zeta = -0.01$ and a dispersion $\sigma_{\Delta\zeta} = 0.10$. The dispersion is however a strong function of the spectral subtype, and it decreases significantly at later subtypes. Splitting the stars in three groups, we find the mean offsets and dispersions ($\Delta\zeta, \sigma_{\Delta\zeta}$) to be $(-0.086, 0.244)$ for subtypes K7.0-M0.5, $(-0.011, 0.103)$ for subtypes M1.0-M2.5, and $(0.008, 0.036)$ for subtypes M3.0-M5.5. Assuming that stars do not show significant variability in those bands, we adopt the dispersions as estimates of the measurement errors on ζ . It is clear from Figure 11 that early type stars should have larger uncertainties in ζ because of the convergence of the iso- ζ lines. The best leverage for estimating metallicities from the TiO and CaH bandheads is at later types when the molecular bands are well developed.

The overall distribution of ζ values as a function of spectral subtype also shows a decrease in the dispersion as a function of spectral type (Figure 12, bottom panel). In early-type dwarfs (K7.0-M0.5), the scatter in the ζ values is relatively large, with $\sigma_\zeta \simeq 0.174$, it drops to $\sigma_\zeta \simeq 0.100$ for subtypes M1.0-M2.5, and to $\sigma_\zeta \simeq 0.059$ for subtypes M3.0-M5.5. Note that the scatter in the M3.0-M5.5 bin is a factor 2 larger than the estimated accuracy of the ζ for that range, as estimated above. We suggest this to be evidence of an intrinsic scatter in the ζ values for the stars in our sample, which we allege

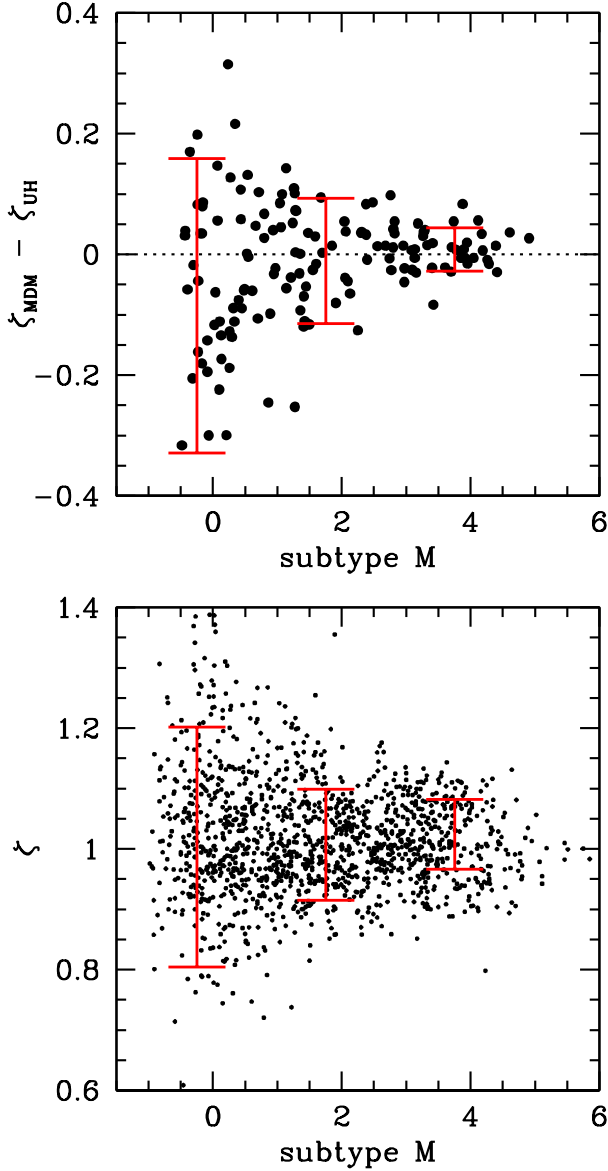


FIG. 12.— The ζ parameter as a function of spectral subtype. Top: difference in ζ for the same stars measured at the two observatories (MDM and UH). The scatter provides an estimate of the measurement error on ζ , which is significantly larger at earlier subtypes. Bottom: adopted values of ζ for all the stars in the survey. The larger scatter at subtypes M2 and earlier can be fully accounted by the measurement errors. The scatter at subtypes M3 and later is larger than the measurement error, and is thus probably intrinsic and is evidence for intrinsic metallicity scatter in the solar neighborhood.

to be the signature of a metallicity scatter. If we subtract in quadrature the 0.035 measurement error on ζ , we estimate the intrinsic scatter to be ≈ 0.05 units in ζ . This intrinsic scatter, which presumably affects all subtypes equally, is unfortunately drowned in the measurement error at earlier subtypes ($< \text{M3}$).

5.2. Comparison with other metallicity diagnostics

To test our ζ as a tracer of metallicity for dM stars from M3 to M6, we compared the values to two recent $[\text{Fe}/\text{H}]$ calibration techniques for M dwarfs with solar metallicities. First, we used the photometric calibration of Neves et al. (2012), which is based on optical-to-infrared color V-K and absolute

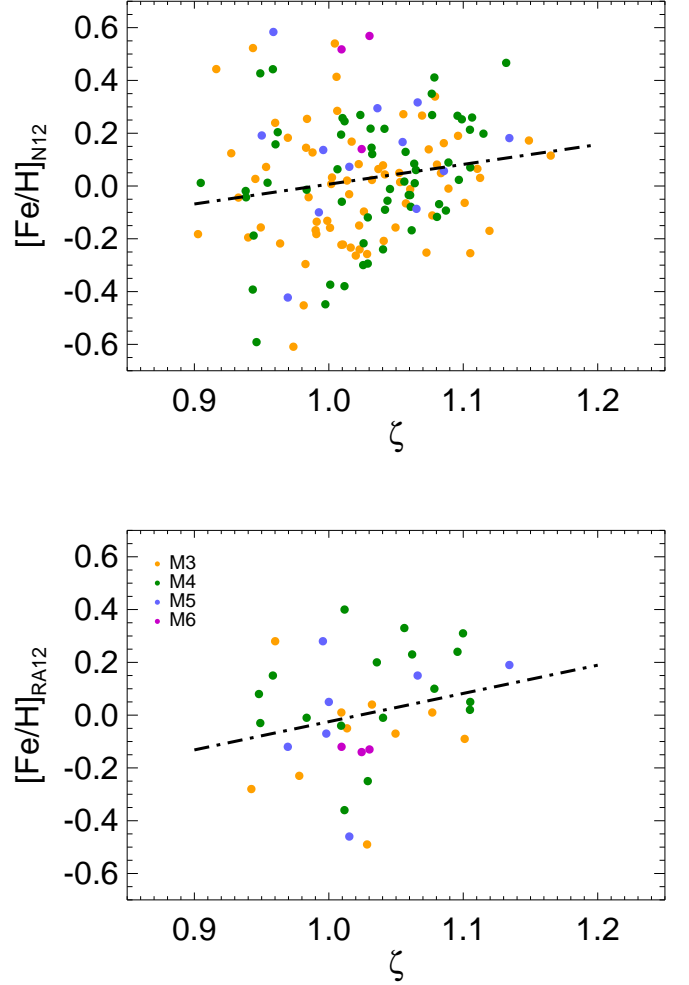


FIG. 13.— Comparison between the ζ parameter values and independent metallicity measurements for subsets of M dwarfs in our survey. Top panel compares our ζ to the $[\text{Fe}/\text{H}]$ estimated from the (V-K, M_K) calibration of Neves et al. (2012) for the same stars. Bottom panel compares our ζ values to the $[\text{Fe}/\text{H}]$ estimated from the infrared K-band index by Rojas-Ayala et al. (2012). Both distribution show weak positive correlations.

magnitude M_K . The method is sensitive to small variations in V-K/ M_K and thus requires an accurate, geometric parallax. A total of 143 stars in our sample have parallaxes, and thus can have their metallicities estimated with this method. Figure 13 (top panel) plots the estimated $[\text{Fe}/\text{H}]$ as a function of ζ for those 143 stars. The distribution shows significant scatter, but we find a weak correlation of $[\text{Fe}/\text{H}]$ with ζ , which we fit with the relationship:

$$[\text{Fe}/\text{H}]_{\text{N12}} = 0.750\zeta - 0.743. \quad (19)$$

Stars are scattered about this relationship with a $1\text{-}\sigma$ dispersion of 0.383 dex. One drawback of the photometric metallicity determination is that it assumes the star to be single. Unresolved double stars appear overluminous at a given color, and will thus be determined to be metal-rich. If there are many unresolved doubles in our catalog, this would increase the scatter in Figure 2; stars with $[\text{Fe}/\text{H}]_{\text{N12}} > 0.4$ could indeed be unresolved doubles.

Next, we retrieve metallicity measurements from Rojas-Ayala et al. (2012), who estimated $[\text{Fe}/\text{H}]$ based on the spectroscopic calibration from infrared K-band atomic features. Their list has 37 stars in common with our survey.

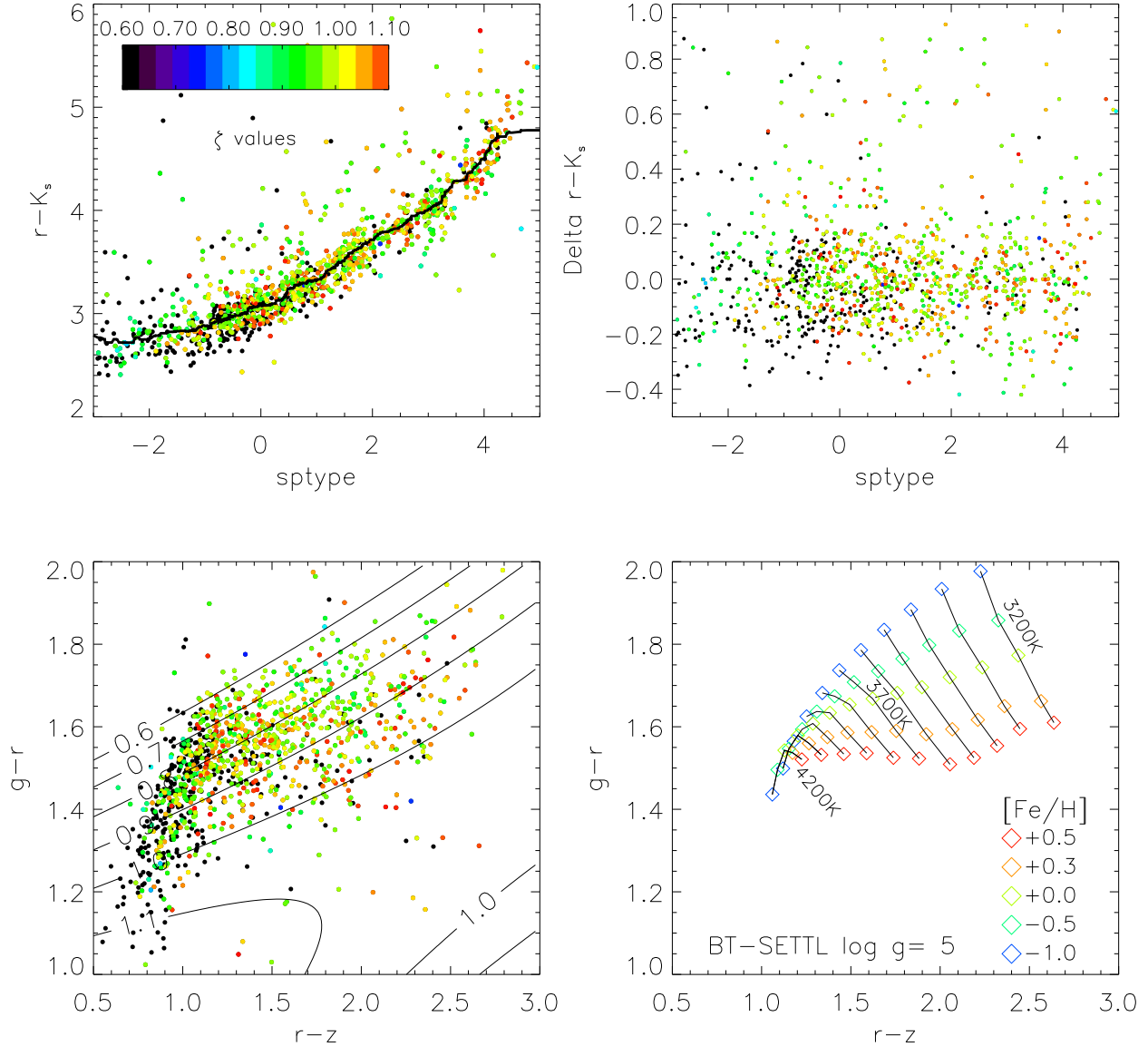


FIG. 14.— SDSS photometry of M dwarf stars synthesized from SNIFS spectra and transmission functions convolved with unit airmass. Upper left: $r-K_s$ (where K_s is from the 2MASS point source catalog) against M spectral subtype (where K7=−1 and K5=−2). Points are colored by the ζ parameter, which measures TiO/CaH ratio and is a metallicity diagnostic in the optical. The ζ values are undefined for late K stars, which are plotted as black points. The black curve is a running median (N=81). Upper right: difference of $r-K_s$ with respect to the running median vs. spectral type, showing no obvious correlation with ζ . Lower left: $g-r$ vs. $r-z$, showing an apparent correlation between these colors ζ . The contours are the empirical function for ζ derived by West et al. (2011). Lower right: SDSS $g-r$ vs. $r-z$ colors generate by the PHOENIX/BT-SETTL model (Allard, Hauschildt, & Schweitzer 2000) for $\log g=5$, $T_{\text{eff}}=3500\text{K}-4200\text{K}$, and five different values of the metallicity as noted in the legend. The model predicts the more metal-rich M dwarfs to have *bluer* $g-r$ colors, while being redder in $r-z$. The color dependence on metallicity is most pronounced in late-type stars, and nearly vanishes at K7/M0.

The $[Fe/H]$ values are plotted as a function of our ζ values in the bottom panel of Figure 13. Again there is significant scatter, but we also find a weak correlation which we fit with the relationship:

$$[Fe/H]_{\text{RA12}} = 1.071\zeta - 1.096, \quad (20)$$

about which there is a dispersion of 0.654 dex. The statistics are relatively poor at this time, and more metallicity measurements in infrared bands would be useful.

The weak correlation found in both distribution is interesting in itself. Using a sample of stars spanning a wide range of metallicities and ζ values, including metal-poor M subdwarfs, extreme subdwarfs (esdM), and extremely metal-poor ultra-

subdwarfs (usdM), Woolf, Lépine, & Wallerstein (2009) determined a relationship of the form $[Fe/H] = -1.685 + 1.632\zeta$, over the range $0.05 < \zeta < 1.10$. All the stars in the two distributions from the present survey have ζ values between ~ 0.9 and ~ 1.2 , and thus represent the metal-rich end of the distribution. The weak correlation and low slopes may indicate that the relationship reaches a plateau and levels off at the high metallicity end. More accurate measurement of both ζ and Fe/H will be needed to corroborate this trend.

5.3. The one M subdwarf: PM 120050+5426 (V1513 Cyg)

The primary purpose of the ζ parameter is the identification of metal-poor M subdwarfs, for which it has already proven

effective. By definition, M subdwarfs are stars with $\zeta < 0.82$ (Lépine, Rich, & Shara 2007). Though we have a few stars with values close to this limit or marginally under, only one star clearly stands out as a possible M subdwarf: the star PM I20050+5426 (= Gl 781) which boasts a $\zeta = 0.58$, well within the M subdwarf regime. The star also clearly stands out in Figure 11 where it lies noticeably below the main locus at $\text{TiO}_5 \simeq 0.75$.

This star is V1513 Cyg, a nearby M subdwarf Gizis (1997) associated with the Galactic halo (Fuchs & Jahreiss 1998) but notorious for being a flaring star, with chromospheric activity due not to young age but to the presence of a low-mass companion on a close orbit (Gizis 1998). Our own spectrum indeed shows a relatively strong line of $H\alpha$ in emission, which is extremely unusual for an M subdwarf. It is an interesting coincidence that the brightest M subdwarf in the northern sky should turn out to be a peculiar object.

In any case, because the TiO molecular bands are weaker in M subdwarfs than they are in M dwarfs, the use of TiO spectral indices for spectral classification leads to underestimates of their spectral subtype. The convention is to base the classification mainly on the strengths of the CaH bandheads (Gizis 1997; Lépine, Rich, & Shara 2003, 2007). We adopt the same convention here, and recalculate the subtype from the mean of Equations 6 and 7 only (CaH2 and CaH3 indices). We thus classified PM I20050+5426 as an sdM2.0, a half-subtype later than the sdM1.5 classification suggested by (Gizis 1997).

5.4. Photometric dependence on metallicity

A prediction of current atmospheric models is that metallicity variations in M dwarfs yield significant variations in optical broadband colors. The metal-poor M subdwarfs have in fact long been known to have bluer V-I colors than the more metal rich M dwarfs of the same luminosity (Monet et al. 1992; Lépine, Rich, & Shara 2003). The bluer colors are due to reduced TiO opacities in the optical, which make the spectral energy distribution of M subdwarfs closer to that of a blackbody, while the metal-rich M dwarfs display extreme red colors.

Interestingly, the SDSS $g-r$ color index shows the opposite trend, and is bluer in the more metal-poor stars. This is because the TiO bands very strongly depress the flux in the 6000Å–7000Å (r-band) range, an effect which in fact makes the metal-rich M dwarfs degenerate in $g-r$, as the increased TiO opacities in cooler stars balance out the reduced flux in g from lower T_{eff} . This effect is much weaker in metal-poor stars due to the reduced TiO opacity, which makes metal-poor stars go redder as they are cooler, as one would normally expect. This has been observed in late-type M subdwarfs, which have significantly redder color than field M dwarfs (Lépine & Scholz 2008). The color dependence of M dwarfs/subdwarfs on metallicity is also predicted by atmospheric models. Figure 14 (bottom-right panel) shows the predicted $g-r$ and $r-z$ colors from the PHOENIX/BT-SETTL model of Allard, Hauschildt, & Schweitzer (2000). The models corroborate observations and predict redder $g-r$ colors in metal-poor stars.

Although $ugriz$ photometry is not available for our stars (all of them are too bright and saturated in the Sloan Digital Sky Survey), it is possible to use the well-calibrated SNIFS spectrophotometry to calculate synthetic broadband riz magnitudes for the subset of stars observed at UH. We first examine any possible correlation between the optical to infrared

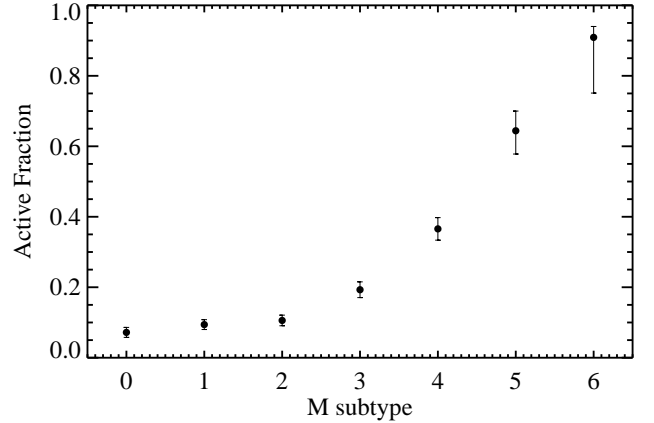


FIG. 15.— Fraction of active stars as a function of the spectral subtype M. The rise at later subtypes is consistent with earlier studies of field M dwarfs. The fraction level at later subtype is however higher than in the SDSS spectroscopic catalog.

$r-K_s$ color (taken as a proxy for V-I) and the ζ index. Figure 14 plots $r-K_s$ as a function of spectral subtype, with the dots color-coded for the ζ values of their associated M dwarf (top-left panel). We find a tight relationship between $r-K_s$ and spectral subtype, which we fit using a running median. The residuals are plotted in the top-right panel, and show no evidence of a correlation with ζ . There are a significant number of outliers with redder $r-K_s$ colors than the bulk of the M dwarfs: these likely indicate systematic errors in estimating the synthetic r band magnitudes. The absence of any clear correlation suggests that an optical-to-infrared color such as $r-K_s$ is not sensitive enough to detect small metallicity variations, at least at the metal-rich end.

The synthetic $g-r$ and $r-z$ colors are plotted in Figure 14 (lower-left panel). The redder stars ($r-z > 1.2$) show a wide scatter in $g-r$, on the order of what is predicted for stars with a range of metallicities $-0.5 < [Fe/H] < 0.5$. Though we do not find a clear trend between the synthetic $g-r$ colors and the ζ values measured in the same stars, the high- ζ stars (red and orange dots on the plot) do seem to have lower values of $g-r$ on average than the low- ζ ones (green dots). The trend is suggestive of a metallicity link to both the $g-r$ colors and the ζ values, and should be investigated further with data of higher precision.

6. CHROMOSPHERIC ACTIVITY

To evaluate the presence of $H\alpha$ in emission in our M dwarfs, we used the $H\alpha$ equivalent width index EWHA defined as:

$$EWHA = 100 \left[1 - \frac{14 \int_{6557.61}^{6571.61} S(\lambda) d\lambda}{100 \left(\int_{6500}^{6550} S(\lambda) d\lambda + \int_{6575}^{6625} S(\lambda) d\lambda \right)} \right], \quad (21)$$

where $S(\lambda)$ is the observed spectrum. The EWHA index measures the flux in a region (6557.61Å–6571.61Å) which includes the $H\alpha$ line, in relation to a pseudo-continuum region spanning 6500Å–6550Å and 6575Å–6625Å; the calculation provides a value in units of wavelength (Å) like the traditional equivalent width. Note that for an $H\alpha$ line in emission, values of the EWHA index are negative, following convention. Assuming the W1-W2 region to measure the true spectral continuum, then the EWHA index would measure the true equivalent width of $H\alpha$. As it turns out, the W1–W2 region

TABLE 6
SURVEY STARS: DISTANCES, KINEMATICS, AND ACTIVITY.

Star name	π_{trig} ''	π_{phot} ''	π_{spec} ''	U km s ⁻¹	V km s ⁻¹	W km s ⁻¹	EWHA Å	H α active	Xray active	UV active
PM I00006+1829	-	-	-
PM I00012+1358S	...	0.030 \pm 0.008	0.028 \pm 0.008	-13.9	12.1	...	0.41	-	-	-
PM I00033+0441	0.0342 \pm 0.0032	0.031 \pm 0.008	0.030 \pm 0.009	8.5	-6.8	...	0.39	-	-	-
PM I00051+4547	0.0889 \pm 0.0014	0.078 \pm 0.021	0.083 \pm 0.024	-38.2	...	-15.9	0.47	-	-	-
PM I00051+7406	-	-	-
PM I00077+6022	...	0.078 \pm 0.031	0.091 \pm 0.027	-15.1	...	-4.4	-3.11	Y	-	-
PM I00078+6736	...	0.046 \pm 0.012	0.055 \pm 0.016	5.1	...	-8.5	0.39	-	-	-
PM I00081+4757	...	0.071 \pm 0.028	0.061 \pm 0.018	7.9	...	1.8	-2.93	Y	-	Y
PM I00084+1725	0.0460 \pm 0.0019	0.040 \pm 0.011	0.040 \pm 0.012	11.2	0.7	...	0.41	-	-	-
PM I00088+2050	...	0.078 \pm 0.031	0.080 \pm 0.024	9.5	...	-10.1	-4.64	Y	-	Y
PM I00110+0512	0.0233 \pm 0.0038	0.032 \pm 0.009	0.031 \pm 0.009	-48.5	-14.3	...	0.35	-	-	-
PM I00113+5837	-	-	-
PM I00118+2259	...	0.055 \pm 0.022	0.054 \pm 0.016	-3.0	...	-16.7	0.30	-	Y	-
PM I00125+2142En	0.0358 \pm 0.0028	0.023 \pm 0.006	0.024 \pm 0.007	-5.9	...	-32.5	0.44	-	-	-
PM I00131+7023	...	0.037 \pm 0.010	0.037 \pm 0.011	-6.2	...	16.8	0.37	-	-	-

often has a higher mean flux than the W3–W4 region without the H α emission component, which means that the EWHA index systematically underestimate the equivalent width of the H α line. The index is however reproducible and more convenient for automated measurement than, e.g. manual evaluation of the equivalent using interactive software such as IRAF.

The EWHA index has been measured for all spectra in our sample, and used to flag active stars. Following West et al. (2011), we define a star to be chromospherically “active” if EWHA < -0.75, which usually corresponds to a clearly detectable H α line in emission. Values of the EWHA index are listed in Table 6. Under the above criterion, 174 M dwarfs in our survey are considered active.

The fraction of stars that are active at each spectral type is shown in Figure 15, with error bars computed from the binomial distribution. The increase in the active fraction with spectral type is consistent with previous studies (West et al. 2004, 2008; Kruse et al. 2010; West et al. 2011), although our active fractions are higher at each subtype. This discrepancy is likely caused by the magnitude limit imposed in our survey: our objects are all nearby, with relatively small distances from the Galactic plane (see Section 7), which makes them statistically younger, as demonstrated in West et al. (2011). The active fractions for our stars are closer to the active fractions for the stars in the nearest Galactic height bins from that study.

Another chromospheric activity diagnostic in M dwarfs is the detection of X-rays. M dwarfs that are X-ray bright are often young, and this has been used to identify members of nearby young moving groups (e.g., Gaidos 1998; Zuckerman et al. 2001; Torres et al. 2006). Most recently, Shkolnik et al. (2009) and Schlieder et al. (2012) used the ratio of *ROSAT* X-ray flux to 2MASS *J* or *K*-band flux to identify candidate members of young moving groups. This technique is effective for objects less than 25 pc away Shkolnik et al. (2009), which includes a large fraction of our sample. The Lépine & Gaidos (2011) catalog, from which our targets are drawn, was already cross-matched to the *ROSAT* All-Sky Bright Source Catalog (Voges et al. 1999) and the *ROSAT* All-Sky Survey Faint Source Catalog (Voges et al. 2000).

We have computed the X-ray flux for our survey stars from the measured count rate and hardness ratio (HR1) using the prescription in Schmitt, Fleming, & Giampapa (1995). Figure 16 shows the distribution of X-ray flux as a function of *V*–*K* color, for the 288 M dwarfs with *ROSAT* detections.

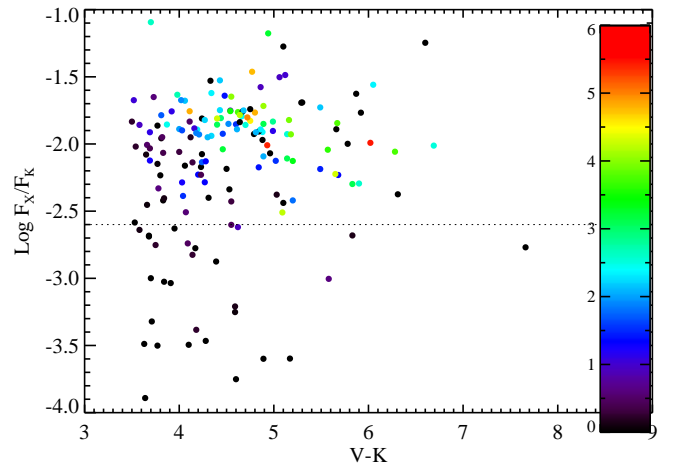


FIG. 16.— X-ray luminosity normalised by the flux in the infrared *K_s* band, plotted as a function of the optical-to-infrared color *V*–*K*, for stars in our sample which have counterparts in the *ROSAT* all-sky points source catalog. The color scheme shows the H α equivalent width; active stars are found to have large X-ray flux, as expected from chromospheric activity.

Dots are color-coded according to the strength of the H α emission, as measured by the EWHA index. Some 152 of the X-ray sources are considered active based on their EWHA values. As expected, M dwarfs with strong H α emission also tend to be X-ray bright. Objects with $\log F_X/F_K > -2.6$ (above the dashed line in Figure 16) are considered bright enough in X-ray to qualify as chromospherically active, as suggested by Schlieder et al. (2012). Some 152 of the X-ray sources are considered active based on their EWHA values; all of them also qualify as active stars based on their X-ray fluxes. On the other hand, 53 M dwarfs identified as active based on X-ray flux do not display significant H α emission in our spectra; most of them tend to be earlier M dwarfs, in which H α emission is not as easily detected as in later type objects because of their higher continuum flux near $\lambda 6563$. There are also 22 stars in our survey which are active based on H α but are not detected by *ROSAT*. This suggests that only two thirds of the “active” stars will be diagnosed as such from both X-ray and H α emission, while the other third will show only either. This could be due to variability in both X-ray and H α emission or, in the case of the X-ray flux, be the result of non-uniform sky-coverage by *ROSAT*.

Active stars can also be identified from ultra-violet excess,

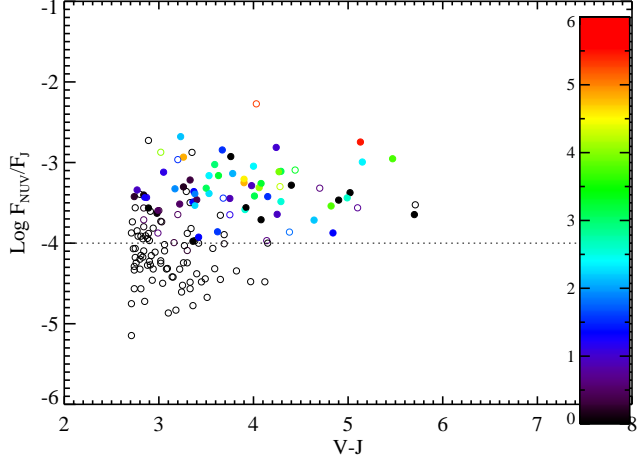


FIG. 17.— Normalized near-UV flux as a function of the optical-to-infrared $V-K_s$ color. The color scheme shows the strength of the $H\alpha$ equivalent width. Closed circles shows stars identified as active based on X-ray emission, closed circles shows stars with low or no detection in ROSAT.

as suggested in Section 3.4. Shkolnik et al. (2011) showed that *GALEX* UV fluxes can identify young M dwarfs in nearby moving groups, and can identify active stars to larger distances. Figure 17 shows the *GALEX* NUV to 2MASS J flux ratio for the objects with UV detections. The dashed line shows the selection criteria of Shkolnik et al. (2011). Dot colors represent the EWHA index values for the stars, while filled circles indicate objects with $\log F_X/F_K > -2.6$, i.e. stars whose X-ray flux does not identify them as being active. Overall, there is a good correspondence between the different activity diagnostics. However, there are some stars identified as active based on UV flux that are not identified as such from their X-ray and/or $H\alpha$ emission. Again this suggests that a complete identification of active M dwarfs in the solar vicinity may require a combination of diagnostic features.

In any case our survey, with combines X-ray, UV, and $H\alpha$ diagnostics, provides a valuable subset for identifying low-mass young stars in the solar neighborhood, and may potentially yield new members of young moving groups, or the identification of new moving groups. The last three columns in Table 6 display flags for stars found to be active from either $H\alpha$, X-ray, or UV flux. The flag indicates activity by a “Y”. Absence of a flag does not necessarily indicate no sign of activity: the *GALEX* survey does not cover the entire sky, and the ROSAT X-ray survey is not uniform in sensitivity, so a non-detection in either does not indicate quiescence. Activity diagnostics could also be time-variable; however there is a good correlation between the different diagnostics. We flag 173 stars as active based on $H\alpha$, 40 based on X-ray emission, and 171 based on UV excess. Overall, 252 stars are assigned one or more activity flags: 17 stars have all three flags on, 98 stars get two flags, and 137 get only one.

7. SPECTROSCOPIC DISTANCES

Astrometric parallaxes are available for 626 of the stars in our sample, spanning the full range of colors and spectral subtypes. We combine these data with our spectroscopic measurements to re-evaluate photometric and spectroscopic distances for M dwarfs. Absolute visual magnitudes M_V are calculated and are plotted against both $V-J$ color and spectral subtype in Figure 18. Individual stars are marked with black dots, and the solid red lines are the best-fit second order polynomials. range of the stars in half-subtype bins. The equa-

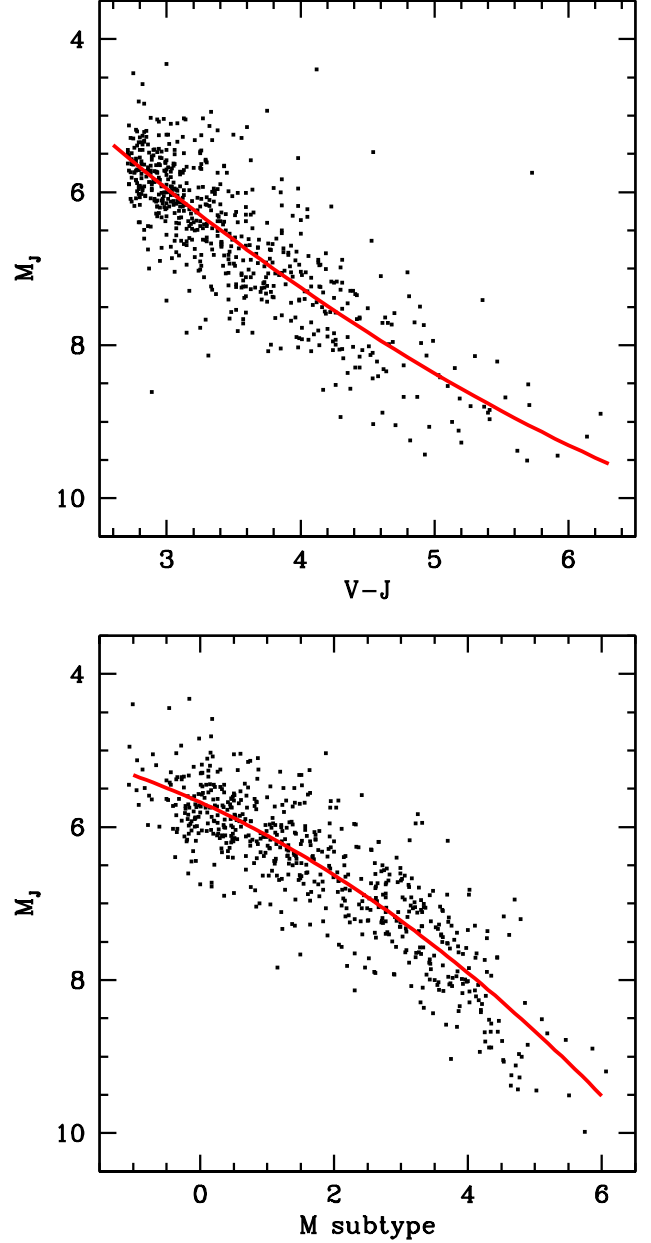


FIG. 18.— Absolute visual (M_V) and infrared (M_J) magnitudes for the 495 stars in our survey for which geometric parallax measurements exist in the literature. Top panels: absolute magnitudes against $V-J$ color, which follow the color-magnitude relationship use in Lépine & Gaidos (2011) to estimate photometric distances. Center panels: absolute magnitudes as a function of spectral subtype, based on the spectral classification from template-fit described in this paper. Bottom panel: absolute magnitude as a function of the CaH2+CaH3 spectral index.

tions for the fits, where spT is the spectral type (K7 is -1 and M0=0, etc) are:

$$M_J = 1.001 + 1.918(V-J) - 0.089(V-J)^2 \quad (22)$$

$$M_J = 5.675 + 0.394(spT) + 0.041(spT)^2 \quad (23)$$

where SpT are the spectral types, and with the least-squares fit performed after exclusion of 3-sigma outliers. The 1σ dispersion about these relationships are comparable, with 0.56 mag for $(M_J, V-J)$, and 0.59 mag for (M_J, SpT) . However, the dis-

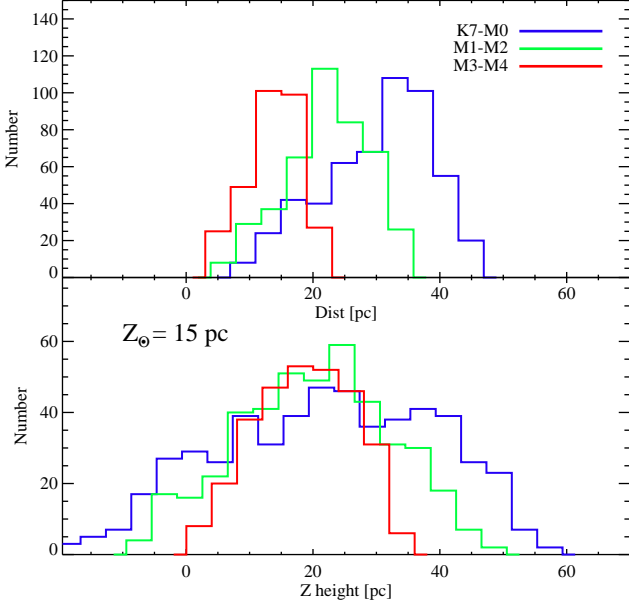


FIG. 19.— Top: distribution of spectroscopic distances for the stars in our survey, shown for three ranges of spectral subtypes. Bottom: distribution of Galactic scale heights for the same stars, assuming that the Sun is hovering 15 pc above the Galactic midplane. As expected from our magnitude-limited sample, stars of later spectral subtypes (and lower luminosity) are found at shorter distances. Our survey samples a region well within the Galactic thin disk.

person is a function of spectral type for (M_J , SpT) because of the change in the slope of the relationship one goes from shallow to steep from early-type M to late-type M; spectral subtype thus provides a better leverage for absolute magnitude in early type stars. The dispersion about the $M_J = M_J(\text{SpT})$ relationship is 0.52 mag for subtypes K7-M2, but it is 0.73 mag for subtypes M3-M6. This suggests that spectroscopic distances are marginally more accurate than photometric distances in early-type stars, but that the photometric distances are more accurate in late-type stars. Using spectroscopic distances for K7-M2 stars would provide a 1σ uncertainty of $\pm 27\%$ on the distance (the uncertainty would be $\pm 40\%$ for M3-M6 stars). Photometric distances estimated from (V,V-J) generally yield uncertainties of $\pm 30\%$ on the distance. Photometric and spectroscopic parallaxes, estimated from the above relationships, are listed in Table 6.

Figure 19 shows the distribution of photometric distances for our complete sample using Equation 23 and the $M_J = M_J(V-J)$ color-magnitude relationship. The spectral subtypes are plotted in separate colors and show that the earlier-type stars, which are intrinsically brighter, are systematically further away than the later-type stars. We also plot the Galactic height of the stars in our sample, adopting a Galactic height of 15 pc for the Sun (Cohen 1995; Ng et al. 1997; Binney, Gerhard, & Spergel 1997). It is clear that our survey is largely contained within the thin disk, and barely extends south of the midplane.

7.1. Kinematic analysis

Accurate radial velocities are not available for most of the stars in our sample, which prevents us from calculating the full (U,V,W) components of motion for each individual star. However, it is possible to use the distance measurements/estimates and proper motion values to evaluate two of

these components for each star. More specifically, we can calculate the (U,V,W) components by assuming that the radial velocities $R_V = 0$. In addition, we can calculate the (X,Y,Z) positions of the stars in the Galactic reference frame, from the distances and sky coordinates. For stars with the largest component of position in +X or -X, the radial velocity mostly contribute to U, and has minimal influence on the values of V and W. Likewise stars with the largest component of position in +Y or -Y (+Z or -Z) make good tracers of the velocity distribution in U and W (U and V). We use this to assign (U,V) or (U,W) or (V,W) velocities to each of the three subsets.

Estimated values of the components of velocity are listed in Table 6. For each star, one of the components is missing, which is the component that would most depend on the radial velocity component based on the coordinates of the star. The other two components are estimated only from proper motion and distance. For the distance, we use the trigonometric parallax whenever available; otherwise we use the most reliable of either the spectroscopic or photometric distance (from estimated errors).

The resulting velocity distributions are displayed in Figure 20. We measure mean values of the velocity components using all allowable values and find:

$$\langle U \rangle = -8.0 \text{ kms}^{-1}, \sigma_U = 32.7 \text{ kms}^{-1},$$

$$\langle V \rangle = -16.9 \text{ kms}^{-1}, \sigma_V = 22.8 \text{ kms}^{-1},$$

$$\langle W \rangle = -6.8 \text{ kms}^{-1}, \sigma_W = 19.2 \text{ kms}^{-1}.$$

These are remarkably similar to the moments of the velocity components calculated by Fuchs et al. (2009) for SDSS stars of the Galactic thin disk, and which are $\langle U \rangle = -8.6$, $\sigma_U = 32.4$, $\langle V \rangle = -20.0$, $\sigma_V = 23.0$, and $\langle W \rangle = -7.1$, $\sigma_W = 18.1$. The agreement suggests that our distance estimates are reasonably accurate.

We note that the stars of our catalog that were previously part of the CNS3 and stars with measured trigonometric parallaxes (e.g. from the Hipparcos catalog) tend to have larger velocity dispersions, with $(\sigma_U, \sigma_V, \sigma_W) = (38.4, 25.9, 23.1)$, while the newer stars have $(\sigma_U, \sigma_V, \sigma_W) = (26.2, 19.4, 15.3)$. The difference could be due to systematic underestimation of the photometric/spectroscopic distances, but a more likely explanation is that the CNS3 and parallax subsample suffers from proper motion selection. This is because most of the CNS3 stars and M dwarfs monitored with Hipparcos were selected from historic catalogs of high proper motion stars, which have a higher limit than the SUPERBLINK proper motion catalog used in the LG2011 selection. This kinematic bias means that the current subset of M dwarfs monitored for exoplanet programs suffers from the same kinematic bias, which could possibly introduce age and metallicity selection effects.

Active stars, on the other hand, are found to have significantly smaller dispersions in velocity space. All 252 stars with at least one activity flags (i.e. stars found to be active either from H α , X-ray flux, or UV excess) are plotted in red in Figure 20. Those active stars have first and second moments:

$$\langle U \rangle = -9.0 \text{ kms}^{-1}, \sigma_U = 24.5 \text{ kms}^{-1},$$

$$\langle V \rangle = -12.6 \text{ kms}^{-1}, \sigma_V = 16.1 \text{ kms}^{-1},$$

$$\langle W \rangle = -6.3 \text{ kms}^{-1}, \sigma_W = 14.9 \text{ kms}^{-1}.$$

The smaller dispersion values suggest that these active stars are significantly younger than the average star in the solar

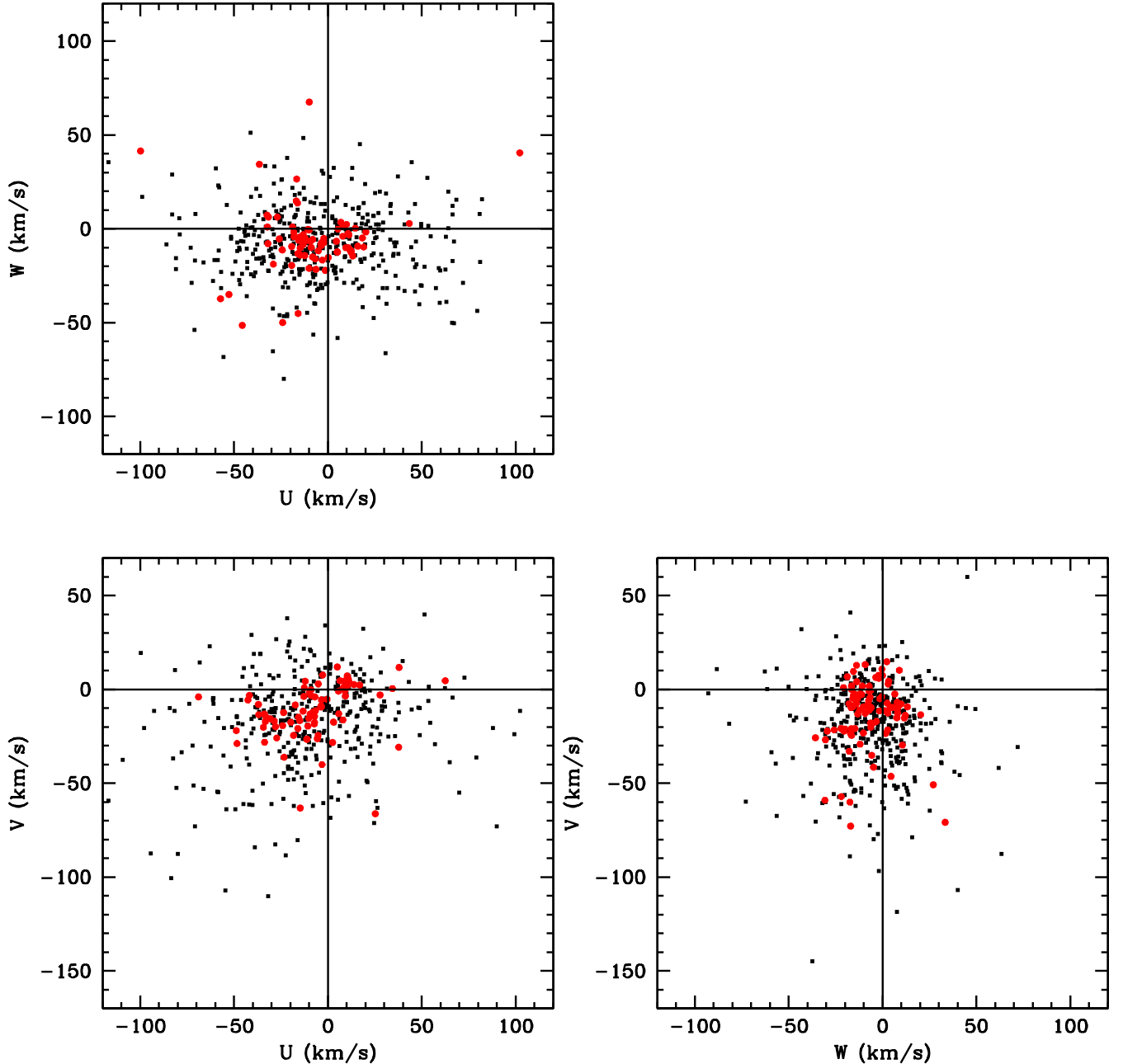


FIG. 20.— Distribution of survey M dwarfs in velocity space, based on photometric distances and proper motions alone. Each star is used in only one panel, which corresponds to the projection in which the radial velocity component locally has the smallest effect on the displayed components. Stars with significant levels of $H\alpha$ emission, i.e. chromospherically active M dwarfs, are labeled in red.

neighborhood. However, we still find active stars with relatively large components of motion, which suggests that young age may not be the only factor contributing to higher chromospheric activity. Spectroscopic follow-up of larger numbers of nearby M dwarfs stars would be useful in drawing a clearer picture of the kinematics of low-mass stars in the solar neighborhood.

8. CONCLUSIONS

We have now compiled spectroscopic data for a nearly complete list of M dwarfs in the northern sky with apparent magnitudes $J < 9$. Our survey identifies a total of 1,403 very bright

M dwarfs. Our new catalog provides spectral subtypes and activity measurements ($H\alpha$ emission) for all stars, as well as a rough indicator of metallicity in the guise of the ζ parameter, which measures the ratio of TiO to CaH bandstrengths. Only one of the stars in the survey is unambiguously identified as a metal-poor M subdwarf (PM I20050+5426 = V1513 Cyg).

Our target stars were identified from the all-sky catalog of bright M dwarfs presented in Lépine & Gaidos (2011). As such, our spectroscopic survey suffers from the same selection effects and completeness issues. The completeness and bias of the SUPERBLINK proper motion survey, from which these stars were selected is discussed a length in Lépine & Gaidos

(2011). In the northern hemisphere, the SUPERBLINK catalog is complete for proper motions $\mu > 40 \text{ mas}^{-1}$. There is a kinematic bias in the catalog which excludes stars with very low transverse motions (in the plane of the sky), but the low proper motion limit means that less than 5% of stars within 50 parsecs of the Sun will be excluded (Figure 1 in Lépine & Gaidos (2011)). As we find in section 7 of this paper, all the M dwarfs in our spectroscopic survey have distances under 50 parsecs, which means our catalog is almost complete. Proper-motion selection may introduce a bias against metal-rich and young stars, however this effect is expected to be small, e.g. a few percent against $[\text{Fe}/\text{H}] = 0$ relative to $[\text{Fe}/\text{H}] = -0.5$ at 45 pc (Gaidos et al. 2012). Nearly all likely members of the Hyades (Perryman et al. 1998), Ursa Majoris (King et al. 2003), and TW Hydrae (Reid 2003) young nearby moving groups have proper motions that exceed 40 mas^{-1} and thus would not be selected against.

Early-type K7-M1 dwarfs have absolute magnitudes $M_J \approx 5.5$, and our $J < 9$ sample thus identifies them to a distance of about 50pc, as confirmed in Figure 19. On the other hand, M4 dwarfs have $M_J \approx 8$ and thus only those at very close distance range ($< 15 \text{ pc}$) will be included in the catalog. Their completeness will however be very high because the proper motion bias excludes less than 1% of the stars within that distance range. In any case, the different survey volumes for early-type and late-type stars means that our survey favors the former over the latter by a factor of about 35 to 1. It is thus no surprise that our spectroscopic catalog is dominated by early-type M dwarfs.

An important result of our survey is the identification of systematic errors in the spectral indices, which measure the strengths of the CaH, TiO, and VO molecular bands. Systematic offsets between data obtained at MDM Observatory and at the University of Hawaii 2.2-meter telescopes, as well as offsets between these and the values measured for the same stars in the Palomar-MSU survey of Reid, Hawley, & Gizis (1995), indicate that these spectral indices are susceptible to spectral resolution and spectrophotometric calibration, such that using the raw measurements may result in systematic errors in evaluating spectral subtypes and the metallicity ζ pa-

rameter. In Section 3.2 we outline a procedure for calculating corrected indices, based on a calibration of systematic offsets between two observatories. A proper calibration requires that large numbers of stars be re-observed every time a new observatory and/or instrumental setup is used, in order to calibrate the offsets and correct the spectral indices. Only the corrected spectral indices can be used reliably in the spectral subtype and ζ relationships, which are calibrated with respect to the corrected values. We adopt the Palomar-MSU measurement as our standard of reference for the spectral indices, and correct our MDM and UH values.

In the end, this catalog provides a useful list of targets for exoplanet searches, especially those based on the radial velocity variation method. Current methods and instruments require relatively bright stars to be efficient, and the stars presented in our spectroscopic catalog constitute targets of choice, having been vetted for background source contamination. Our accurate spectral types will be useful to guide radial velocity surveys and select stars of comparatively lower masses.

We also provide diagnostics for chromospheric activity from H α emission, X-ray flux excess, and UV excess. Besides being useful to identify more challenging sources for radial velocity surveys, they also isolate the younger stars in the census. Follow-up radial velocity observations could tie some of the stars to nearby moving groups, and these objects would be prime targets for exoplanet searches with direct imaging methods.

Acknowledgments

This material is based upon work supported by the National Science Foundation under Grants No. AST 06-07757, AST 09-08419, and AST 09-08406. We thank Greg Aldering for countless instances of assistance with SNIFS, the telescope operators of the UH 2.2m telescope, and Justin Troyer for observing assistance. We thank Bob Barr and the staff at the MDM observatory for their always helpful technical assistance.

REFERENCES

- Aldering, G., et al. 2006, *ApJ*, 650, 510
 Allard, F., Hauschildt, P. H., & Schweitzer, A. 2000, *ApJ*, 539, 366
 Allard, F., Homeier, D., & Freytag, B. 2010, arXiv:1011.5405
 Alpert, N., & Lépine, S. 2011, American Astronomical Society, AAS Meeting #217, #242.11, BAAS, Vol. 43
 Apps, K., Clubb, K. I., Fischer, D. A., et al. 2010, *PASP*, 122, 156
 Asplund, M., Grevesse, N., Sauval, A. J., & Scott, P. 2009, *ARA&A*, 47, 481
 Bacon, R., et al. 2001, *MNRAS*, 326, 23
 Bean, J. L., Seifahrt, A., Hartman, H., et al. 2010, *ApJ*, 713, 410
 Binney, J., Gerhard, O., & Spergel, D. 1997, *MNRAS*, 288, 365
 Bochanski, J. J., et al. 2007, *AJ*, 139, 2679
 Bochanski, J. J., et al. 2010, *AJ*, 139, 2679
 Boyd, M. R., et al. 2011, *AJ*, 142, 92
 Butler, R. P., Johnson, J. A., Marcy, G. W., et al. 2006, *PASP*, 118, 1685
 Casagrande, L., Flynn, C., & Bessell, M. 2008, *MNRAS*, 389, 585
 Cohen, M. 1995, *ApJ*, 444, 874
 Covey, K. R., et al. 2007, *AJ*, 134, 2398
 Covey, K. R., et al. 2008, *AJ*, 136, 1778
 Cutri, R. M., et al. 2003, The 2MASS All-Sky Catalog of Point Sources
 University of Massachusetts and Infrared Processing and Analysis Center (IPAC/California Institute of Technology), Pasadena, CA, USA.
 Dhital, S., et al. 2012, *AJ*, 143, 67
 Dong, S., et al. 2009, *ApJ*, 698, 1826
 Fuchs, B., & Jahreiss, H. 1998, *A&A*, 329, 81
 Fuchs, B., et al. 2009, *AJ*, 137, 4149
 Gaidos, E. J. 1998, *PASP*, 110, 1259
 Gaidos, E., Haghighipour, N., Agol, E., et al. 2007, *Science*, 318, 210
 Gaidos, E., Fischer, D. A., Mann, A. W., & Lépine, S. 2012, *ApJ*, 746, 36
 Gizis, J. E., 1997, *AJ*, 113, 806
 Gizis, J. E., 1998, *AJ*, 115, 2053
 Gliese, W., & Jahreiss, H. 1991, Preliminary Version of the Third Catalogue of Nearby Stars, Astron. Rechen-Institut, Heidelberg
 Irwin, J., Charbonneau, D., Nutzman, P., & Falco, E. 2009, American Institute of Physics Conference Series, 1094, 445
 Isaacson, H., & Fischer, D. 2010, *ApJ*, 725, 875
 Hartman, J. D., Bakos, G. Á., Noyes, R. W., et al. 2011, *AJ*, 141, 166
 Hawley, S. L., et al. 2002, *AJ*, 123, 3409
 Herrero, E., Ribas, I., Jordi, C., Guinan, E. F., & Engle, S. G. 2011, arXiv:1110.5840
 King, J. R., Villarreal, A. R., Soderblom, D. R., Gulliver, A. F., & Adelman, S. J. 2003, *AJ*, 125, 1980
 Kirkpatrick, J. D., Henry, T. H., & McCarthy Jr., D. W. 1991, *ApJ*, 77, 417
 Kruse, E. A., et al. 2010, *ApJ*, 722, 1352
 Henry, T. J., et al. 2006, *AJ*, 132, 2360
 Lantz, B., Aldering, G., Antilogus, P., et al. 2004, *Proc. SPIE*, 5249, 146
 Lépine, S., Rich, R. M., & Shara, M. M. 2003, *AJ*, 125, 1598
 Lépine, S., & Shara, M. M. 2005, *AJ*, 129, 1483
 Lépine, S., 2005, *AJ*, 130, 1247
 Lépine, S., 2008, *AJ*, 135, 2177
 Lépine, S., & Gaidos, E. *AJ*, 142, 138

- Lépine, S., Rich, R. M., & Shara, M. M. 2007, *ApJ*, 669, 1235
- Lépine, S. & Scholz, R.-D. 2008, *ApJ* 681, L33
- Mann, A. W., Gaidos, E., Lépine, S., & Hilton, E. 2012, *ApJ*, 753, 90
- Mayor, M., Bonfils, X., Forveille, T., et al. 2009, *A&A*, 507, 487
- Monet et al. 1992, *AJ*, 103, 638
- Mould, J. R. 1976, *ApJ*, 207, 535
- Mugrauer, M., Vogt, N., Neuhauser, R., & Schmidt, T. O. B. 2010, *A&A*, 523, L1
- Neves, V., Bonfils, X., Santos, N. C., et al. 2012, *A&A*, 538, id.A25
- Ng, Y. K., Bertelli, G., Chiosi, C., & Bressan, A. 1997, *A&A*, 324, 65
- Oke, J. B. 1991, *AJ*, 99, 1621
- Perryman, M. A. C., Brown, A. G. A., Lebreton, Y., et al. 1998, *A&A*, 331, 81
- Quirrenbach, A., Amado, P. J., Mandel, H., et al. 2010, *Pathways Towards Habitable Planets*, 430, 521
- Reid, I. N., Hawley, S. L., & Gizis, J. E. 1995, *AJ*, 110, 1838
- Reid, I. N., Gizis, J. E., & Hawley, S. L. 2002, *AJ*, 124, 2721
- Reid, N. 2003, *MNRAS*, 342, 837
- Reid, I. N., Cruz, K. L., & Allen, P. R. 2007, *AJ*, 133, 2825
- Rojas-Ayala, B., Covey, K. R., Muirhead, P. S., & Lloyd, J. P. 2012, *ApJ*, 748, 93
- Schlieder, J. E., Lépine, S., & Simon, M. 2012, *AJ*, 143, 80
- Schmitt, J. H. M. M., Fleming, T. A., & Giampapa, M. S. 1995, *ApJ*, 450, 392
- Shkolnik, E. L., Liu, M. C., & Reid, I. N. 2009, *ApJ*, 699, 649
- Shkolnik, E. L., Liu, M. C., Reid, I. N., Dupuy, T., & Weinberger, A. J. 2011, *ApJ*, 727, 6
- Sousa, S. G., Santos, N. C., Israelian, G., Mayor, M., & Udry, S. 2010, *A&A*, 533, 141
- Reid, I. N., Hawley, S. L., & Gizis, J. E. *AJ*, 110, 1838
- Reylé, C., Rajpurohit, A. S., Schultheis, M., & Allard, F. 2011, *arXiv:1102.1263*
- Tarter, J. C., Backus, P. R., Mancinelli, R. L., et al. 2007, *Astrobiology*, 7, 30
- Terada, H., Yuji, I., Kobayashi, N., et al. 2008, *Proc. SPIE*, 7014, 103
- Torres, C. A. O., et al. 2006, *A&A*, 460, 695
- van Leeuwen F. 2007, *A&A*, 474, 653
- Voges, W., et al. 1999, *A&A*, 349, 389
- Voges, W., et al. 2000, *IAU Circ.* 7432, 1
- Wang, W., Gully-Santiago, M., Deen, C., Mar, D. J., & Jaffe, D. T. 2010, *Proc. SPIE*, 7739, 146
- West, A. A., et al. 2004, *AJ*, 128, 426
- West, A. A., et al. 2008, *AJ*, 135, 785
- West, A. A., et al. 2011, *AJ*, 141, 97
- Woolf, V. M., Lépine, S., & Wallerstein, G. 2009, *PASP*, 121, 117
- Zuckerman, B., Song, I., Bessell, M. S., & Webb, R. A. 2001, *ApJ*, 562, L87